Composite Structures 351 (2025) 118629

Contents lists available at ScienceDirect

Composite Structures

journal homepage: www.elsevier.com/locate/compstruct

A semi-analytical model for predicting the shear buckling of laminated composite honeycomb cores in sandwich panels

Jasotharan Sriharan [a], Marcelo Dias [a], Sondipon Adhikari [b], Dilum Fernando [a,*]

[a] School of Engineering, University of Edinburgh, EH9 3FG, UK
[b] James Watt School of Engineering, The University of Glasgow, G12 8QQ, UK

ARTICLE INFO

Keywords:
Shear buckling
Honeycomb core
Cellular core
Laminated composite
Sandwich panels
Bend-twist coupling

ABSTRACT

Laminated composite honeycomb cellular core sandwich panels are widely utilized in various industries due to their exceptional stiffness-to-weight ratio and strength characteristics. Current analytical models often simplify honeycomb cores as homogenized continua, effectively predicting stiffness but falling short in capturing crucial failure modes, particularly shear buckling of honeycomb core walls. Existing theoretical studies on shear buckling are limited to isotropic materials and specific honeycomb geometries. While numerical models can simulate cell wall buckling, their computational demands render them impractical for large structures employing sandwich panels. This paper introduces a novel, simplified semi-analytical approach that accurately predicts the shear buckling load of laminated composite honeycomb cellular cores. The model accounts for bend-twist coupling effects and rotational restraints at laminate wall boundaries. To validate the proposed approach, predictions are compared with finite element analysis results for hexagonal honeycomb cores and cores of varying shapes, incorporating diverse fibre lay-up configurations. The findings demonstrate excellent agreement between the proposed approach and finite element analysis, indicating its reliability in predicting shear buckling. This research addresses the gap in existing methodologies by offering a practical and efficient tool for predicting shear buckling in laminated composite honeycomb cores, extending applicability beyond isotropic materials and specific honeycomb geometries. The proposed approach holds promise for optimizing the design and structural integrity of sandwich panels, impacting industries relying on these lightweight and high-performance structures.

1. Introduction

Sandwich panels are widely used in many engineering applications due to their high stiffness-to-weight ratio and strength properties. The honeycomb core is one of the most commonly used core types in sandwich panels, which can be built from a variety of materials ranging from isotropic metal foils to fibre-reinforced composite [1–5]. Localised buckling of the cell walls is a commonly observed failure mode in honeycomb core sandwich panels [6,7]. Optimising geometric designs, material selections, and stability analyses to mitigate local buckling in honeycomb core sandwich panels can serve as a blueprint for advancing mechanical metamaterials, facilitating the development of structures with precisely tailored mechanical properties. While three-dimensional (3D) numerical models can capture localised failures such as shear buckling of core, such models are complex and easily become impractical due to high computational costs when modelling large-scale structures. Often, equivalent homogenised models, where the honeycomb core is represented using its effective stiffness properties [8–10], are adopted in analysing the behaviour of large-scale sandwich structures. While such equivalent models managed to capture the global behaviour of the sandwich structures well, they failed to capture localised failures such as the shear buckling of the honeycomb core.

Shear buckling of the honeycomb core is related to the responses at the local level (stress at each plate), which cannot be calculated directly using the equivalent properties. The stresses at the local level depend on the geometry and material parameters of the core; therefore, the modelling approach must be capable of capturing the local geometric and material parameter variations. Therefore, relationships relating the macro-level responses to the local responses are needed. Only a very limited number of studies are available in the existing literature addressing the issue of the shear buckling of honeycomb cores. In the past, researchers [11–16] have mainly investigated the shear buckling strength of the honeycomb cores with isotropic walls. In most of the theoretical studies [14–16], boundary conditions for the plates were

* Corresponding author.
E-mail address: dilum.fernando@ed.ac.uk (D. Fernando).

https://doi.org/10.1016/j.compstruct.2024.118629
Received 8 June 2024; Received in revised form 30 August 2024; Accepted 4 October 2024
Available online 6 October 2024

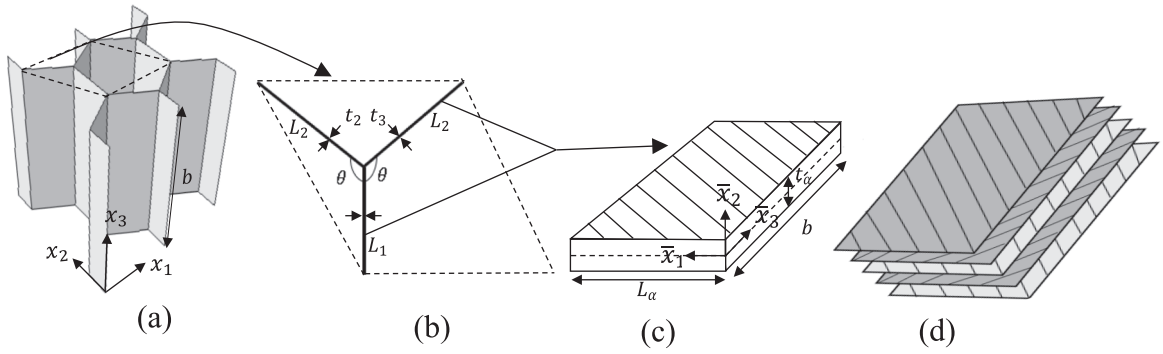

Fig. 1. (a) Typical periodic hexagonal honeycomb core and (b) RVE of hexagonal core fabricated using (c) laminated composite wall having different (d) fibre layer arrangements. Global variables are defined with respect to the (x_1, x_2, and x_3) coordinate system and local variables of each plate are defined with respect to the ($\bar{x}_1$, $\bar{x}_2$, and $\bar{x}_3$) coordinate system.

assumed to be either simply supported or fixed supported. However, the assumption of simply supported condition for the plate edges underestimates the prediction, while the fixed supported assumption overestimates. Shi and Tong [17] have considered the boundary conditions of the plate in between simply supported and fixed by estimating the rotational restraint provided by adjacent plates at the onset of buckling. In most of the studies [14–16], shear buckling strength has been calculated considering shear loading separately in two different principal directions. However, the shear buckling strength of the honeycomb core depends on the effective direction of shear loading when the honeycomb core is subjected to combined transverse shear in two different directions [18]. Some researchers [18–21] have also considered the shear buckling of the honeycomb cores of different shapes. López Jiménez and Triantafyllidis [20] and Qiu et al. [21] proposed analytical models to predict the out-of-plane normal and shear buckling of the honeycomb cores of different shapes, including hexagonal and square cores. The method combines the Bloch wave representation theorem for the eigenmode with the analytical solution of the linearised von Kármán plate equations to analyse the representative volume element (RVE). However, the models proposed in the past do not consider the different material configurations, such as laminated composite for the honeycomb core. In recent studies, many researchers [3–5] have used composite laminates to manufacture various shaped ultralightweight honeycomb cores for weight-sensitive applications. Pathirana et al. [22–24] recently proposed a semi-analytical approach for the out-of-plane compression buckling of composite hexagonal honeycomb core [22] and in-plane shear and compression buckling of corrugated core [23,24]. However, modelling approach to capture the shear buckling of composite honeycomb cores of different shapes is yet to be developed. Considering the potential of composite honeycomb cores of different shapes for various sandwich structure applications, and one of the dominant modes of failure is local shear buckling of the cell walls, it's necessary to have a simplified model to predict the shear buckling of honeycomb cores of different shapes to design and optimise sandwich structures.

This paper presents a semi-analytical model to predict the critical shear buckling load of the laminated composite honeycomb cores of different shapes and material configurations. The proposed approach uses the analysis of the RVE of honeycomb cores together with laminated composite plate buckling theory [25] to predict the critical buckling strain of the laminated composite honeycomb cores. Following the introduction in Section 1, Section 2 of this paper presents the derivations of the semi-analytical model for the shear buckling of the laminated composite wall honeycomb core. Unlike most of the shear buckling solutions for the composite plates [26–31], which do not consider the bend-twist coupling, the shear buckling solution in the proposed approach has been developed considering bend-twist coupling due to the angle-ply laminates. Based on the theoretical solutions, phase failure maps of the hexagonal honeycomb core are plotted for simplified cases such as core with identical laminated walls without bend-twist coupling, etc., and the solutions for the shear buckling load under different shear loadings are discussed in Section 3. In Section 4, theoretical solutions for the honeycomb cores of rectangular and triangular shapes are derived using the proposed methodology. In Section 5, the results from the proposed semi-analytical approach are validated against the results from the finite element (FE) analysis for the laminated composite honeycomb cores of various material configurations.

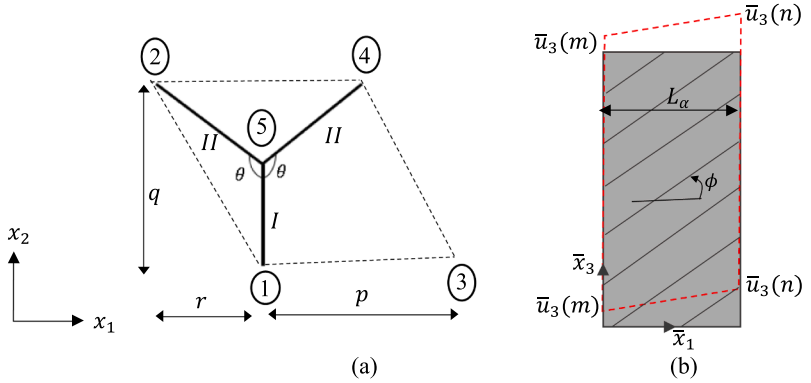

Fig. 2. (a) RVE of the hexagonal core with the nodal numbers and characteristic dimensions (b) deformed shape of the plate under positive shear strain. The positive angle ϕ of the fibre is measured anti-clockwise with respect to the positive direction-$\bar{x}_1$.

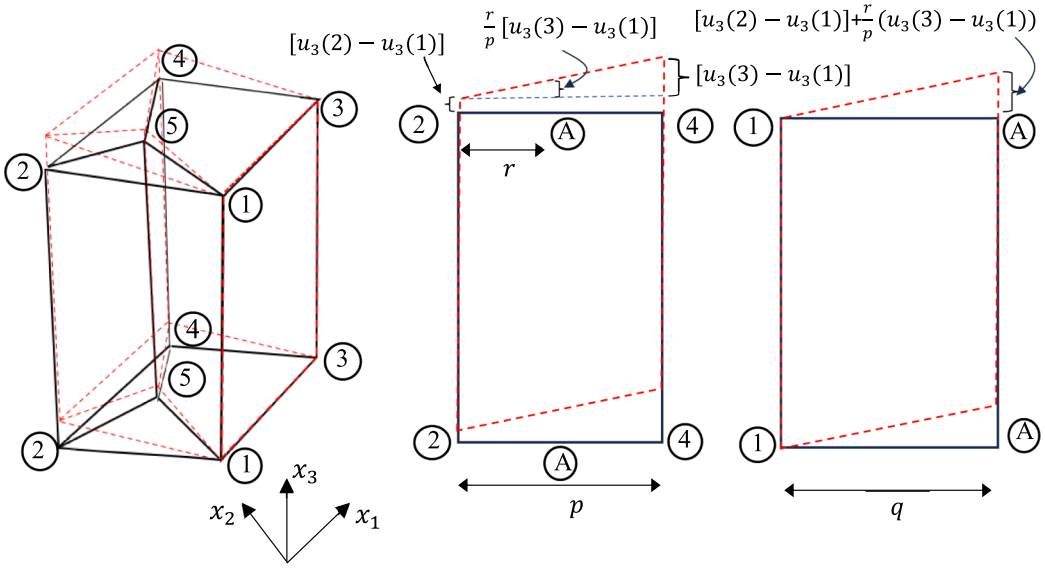

Fig. 3. Diagrammatic illustration of the global transverse shear strains of typical hexagonal core RVE.

2. Proposed approach

Fig. 1(a) shows a typical periodic honeycomb core structure built using laminated composite plates (Fig. 1(c)) having different fibre layer sequences. When flexural loads are applied on sandwich panels consisting of honeycomb core, transverse shear forces are predominantly carried by the honeycomb core [28–31]. While it is possible that honeycomb core cell walls may also carry compression forces, considering core depth is typically much larger than the thickness of the cell walls [31], such compression forces can be taken as negligible compared to transverse shear forces acting on the cell walls. Therefore, only transverse shear forces acting on cell walls are considered in this study. Similar to the assumptions made in existing studies [17], this study also assumes that transverse shear stresses are constant across the depth of the core.

The honeycomb core is considered to fail due to buckling if any of the individual cell walls buckle due to transverse shear stress. Therefore, the shear buckling load of the honeycomb core is defined as the critical global transverse shear strain at which any of the plates buckles first. To determine the critical global transverse shear strain of the honeycomb core, it is necessary to determine the relationship between the in-plane shear strain of the individual plate to the global transverse shear strain of the honeycomb core.

2.1. Determination of shear strain at each plate due to transverse shear strain in the core

To illustrate the proposed approach, a representative volume element (RVE) of a hexagonal core shown in Fig. 1(b) is considered. Displacement field $\boldsymbol{u}$ of the hexagonal core is defined in the global Cartesian coordinate system (x_1, x_2, and x_3) as: $\boldsymbol{u} = \{u_1, u_2, u_3\}^T$, where u_i is component of the displacement in global direction-x_i, and in the local (individual plate) Cartesian coordinate system ($\overline{x}_1, \overline{x}_2$, and $\overline{x}_3$) as: $\boldsymbol{u} = \{\overline{u}_1, \overline{u}_2, \overline{u}_3\}^T$, where $\overline{u}_i$ is component of the displacement in local direction-$\overline{x}_i$.

Each plate of the selected RVE of the hexagonal core (Fig. 2(a)) is analysed for the shear deformation considering the displacement at each node. Each node of the RVE (Fig. 2(a)) is considered to subject to a displacement in direction-x_3 or (or $\overline{x}_3$) due to the applied global transverse shear load on the RVE. Fibre orientations of lamina of the composite plate (Fig. 2(b)) are defined such that the anti-clockwise angle is positive with respect to positive direction-$\overline{x}_1$. The positive direction-$\overline{x}_1$ is defined for the plates *I*, *II*, and *III,* from node 1 to 5, node 5 to 2 and node 5 to 4 respectively. The positive direction-$\overline{x}_3$ is defined always in the positive global direction-x_3. Considering the sign convention assumed here, the positive shear strain of each plate (Fig. 2) is expressed as:

$$\overline{\gamma}^{\alpha} = \frac{\overline{u}_3(n) - \overline{u}_3(m)}{L_{\alpha}}, \tag{1}$$

where $\overline{u}_3(n)$ and $\overline{u}_3(m)$ are the displacements in local direction-$\overline{x}_3$ at the start node-*m* and end node-*n*, respectively of plate-α and $\overline{\gamma}$ is the in-plane shear strain of the plate-α (α refers to plates *I*, *II*, and *III* and L_{α} refers to length of the plate).

The relationship between the in-plane forces and strains for a symmetrically laminated composite laminate (Fig. 2. (b)) can be written using classical laminate theory [25] as:

$$\begin{Bmatrix} \overline{N}_{11} \\ \overline{N}_{33} \\ \overline{F} \end{Bmatrix} = \begin{bmatrix} \overline{A}_{11} & \overline{A}_{13} & \overline{A}_{16} \\ \overline{A}_{13} & \overline{A}_{33} & \overline{A}_{36} \\ \overline{A}_{16} & \overline{A}_{36} & \overline{A}_{66} \end{bmatrix} \begin{Bmatrix} \overline{\varepsilon}_{11} \\ \overline{\varepsilon}_{33} \\ \overline{\gamma} \end{Bmatrix}, \tag{2}$$

where $\overline{N}_{11}$ and $\overline{N}_{33}$ are the in-plane normal forces in direction $\overline{x}_1$ and $\overline{x}_3$, respectively and $\overline{F}$ is in-plane shear force of the laminate; $\overline{\varepsilon}_{11}$ and $\overline{\varepsilon}_{33}$ are the in-plane normal strains and $\overline{\gamma}$ is the shear strain of the laminate; and $\overline{A}_{ij}$ is a component of membrane stiffness matrix of the laminate (*i* and *j* are 1,3,6).

Considering the assumption that the core is subjected to only transverse shear strain, we may also assume that in-plane normal strains $\overline{\varepsilon}_{11}$ and $\overline{\varepsilon}_{33}$ of the walls are equal to zero. Therefore, the relationship between the in-plane shear strain to the shear force of the plate-α can be simplified as:

$$\overline{\gamma}^{\alpha} = \frac{\overline{F}^{\alpha}}{\overline{A}^{\alpha}_{66}}, \tag{3}$$

where $\overline{F}^{\alpha}$ and $\overline{A}^{\alpha}_{66}$ are in-plane shear load and the in-plane section shear stiffness of plate-α, respectively.

In order to find the relationship between the applied transverse shear strain of the honeycomb core and the shear strain at each plate, first, the displacement at each node needs to be determined in terms of the applied transverse shear strain, taking into account the periodic nature of the honeycomb core. Considering the periodic boundary conditions and force equilibrium of the RVE, nodal displacements can be solved to get the strain at each plate due to the applied global strain. Applying the

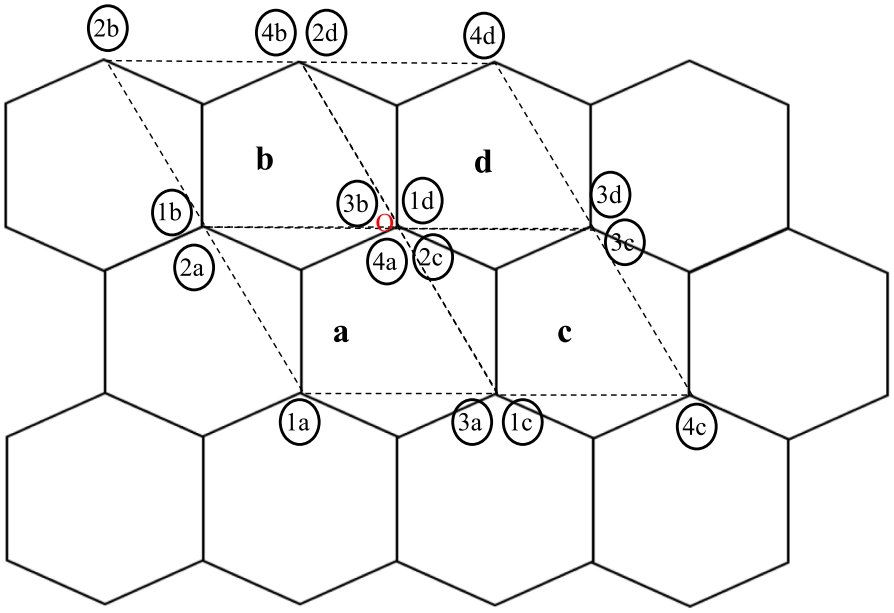

Fig. 4. Repetition of the RVEs to form the periodic honeycomb core.

periodic boundary condition to RVE in Fig. 2(a), we can get the following expression:

$$u_3(3) - u_3(1) = u_3(4) - u_3(2), \tag{4}$$

where $u_3(n)$ is the displacement of node-n in global direction-x_3. RVE is assumed not to undergo any rigid body motions. Therefore, we can write,

$$u_3(1) = 0. \tag{5}$$

The average macroscopic strain of a RVE [32,33] of the periodic structure can be calculated as:

$$\varepsilon_{ij} = \frac{1}{V_{RVE}} \int_V \varepsilon_{ij}^* dV, \tag{6}$$

where ε_{ij}^* and ε_{ij} are the micro-strain and average strain of the RVE, and V_{RVE} is the volume of the RVE. Using Gauss's theorem, the volume average macroscopic shear strain of the RVE can be expressed as an integration of differential displacements around the boundary surfaces of the RVE [32,33] as:

$$\gamma_{ij} = \frac{1}{V_{RVE}} \int_s (u_i n_j + u_j n_i) dS. \tag{7}$$

where n_i is the component of the outward unit normal vector of the boundary surface of RVE.

Using the conditions given in Eq. (5) and average strain of the RVE given in Eq. (7), following relationships can be obtained for the global transverse shear strain (Fig. 3) of the hexagonal core RVE:

$$\gamma_{13} = \frac{u_3(3) - u_3(1)}{p}, \tag{8}$$

$$\gamma_{23} = \frac{u_3(2) - u_3(1)}{q} + \frac{r}{p}\frac{u_3(3) - u_3(1)}{q}, \tag{9}$$

Sum of the forces in all four corner nodes should be zero in RVE. This can be explained considering the repetition of the RVE in Fig. 4. Considering adjacent RVEs a, b, c and d, the resultant force at point O should be zero, which reads as follows:

$$F(1d) + F(2c) + F(4a) = 0, \tag{10}$$

where $F(n)$ is the shear force at node-n.

Considering the adjacent RVEs for the analysis, we can also write:

$$F(1d) = F(1a) \text{ and } F(2c) = F(2a) \tag{11}$$

From Eq. (10) and (11), we will get another equation for the RVE:

$$F(1) + F(2) + F(4) = 0. \tag{12}$$

Resultant force at the internal node of RVE also should be zero, which gives:

$$F(5) = 0. \tag{13}$$

In this scenario, Eq. (13) is not an independent equation because if the local equilibrium of each plate is considered, then Eq. (13) will give the same equation as Eq. (12). The general procedure to formulate the required equations to solve for the displacements of the RVE was outlined above considering the hexagonal honeycomb core which can also be used for honeycomb cores of different shapes.

Now considering the Eqs. (4)-(13), the nodal displacements can be found in terms of geometric and stiffness parameters of the RVE and substituting the results into Eq.(1), the relationships between the applied global shear strains γ_{13} and γ_{23} of the RVE and the shear strain of each plate $\overline{\gamma}^{\alpha}$ of the RVE can be expressed as:

$$\overline{\gamma}^{\alpha} = \gamma_{13} f^{\alpha}, \tag{14}$$

where;

$$f^{I} = \frac{k(\overline{A}_{66}^{II} + \overline{A}_{66}^{III})(L_1 - L_2 cos\theta) + (\overline{A}_{66}^{III} - \overline{A}_{66}^{II})L_2 sin\theta}{\overline{A}_{66}^{I} L_2 + (\overline{A}_{66}^{II} + \overline{A}_{66}^{III})L_1}, \tag{15}$$

$$f^{II} = \frac{k(L_1 - L_2 cos\theta)\overline{A}_{66}^{I} - (L_2\overline{A}_{66}^{I} + 2L_1\overline{A}_{66}^{III})sin\theta}{\overline{A}_{66}^{I} L_2 + (\overline{A}_{66}^{II} + \overline{A}_{66}^{III})L_1}, \tag{16}$$

$$f^{III} = \frac{k(L_1 - L_2 cos\theta)\overline{A}_{66}^{I} + (L_2\overline{A}_{66}^{I} + 2L_1\overline{A}_{66}^{II})sin\theta}{\overline{A}_{66}^{I} L_2 + (\overline{A}_{66}^{II} + \overline{A}_{66}^{III})L_1}, \tag{17}$$

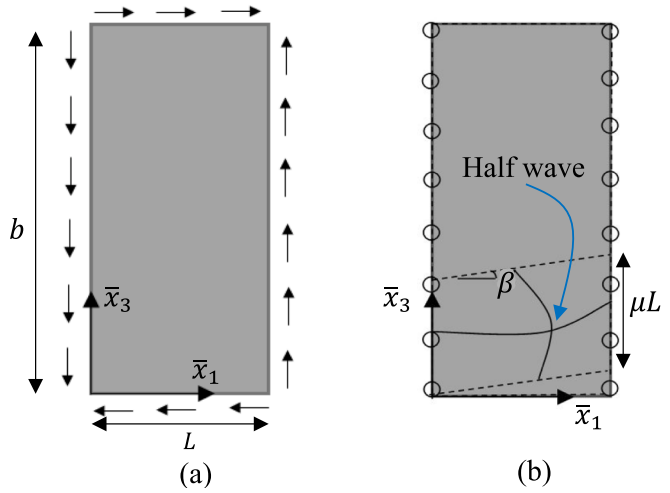

Fig. 5. (a) Composite plate subjected to in-plane shear (b) rotationally restrained plate along longer edges.

and the ratio between the applied shear strain γ_{23}/γ_{13} is k.

Substituting Eq. (14) with Eq. (3), the relationship for the shear strain γ_{13} of the RVE can be written as:

$$\gamma_{13} = \frac{\overline{F}^{\alpha}}{\overline{A}^{\alpha}_{66} f^{\alpha}}. \tag{18}$$

The critical shear buckling load of the honeycomb core is defined as the minimum shear load which requires for any of the plate of RVE to buckle, therefore, the condition to determine the critical shear strain of the hexagonal core can be written as:

$$\gamma_{cr} = min\left\{ \left| \frac{\overline{F}^{I}_{cr}}{\overline{A}^{I}_{66} f^{I}} \right|, \left| \frac{\overline{F}^{II}_{cr}}{\overline{A}^{II}_{66} f^{II}} \right|, \left| \frac{\overline{F}^{III}_{cr}}{\overline{A}^{III}_{66} f^{III}} \right| \right\}. \tag{19}$$

where $\overline{F}^{\alpha}_{cr}$ is the critical shear buckling load of plate-α.

displacement function represents the simply supported boundaries for all the edges and when R becomes 1 then the displacement function implies the clamped longer edges. R could be determined considering the boundary conditions along the rotationally restrained edges.

The boundary conditions along the rotationally restrained edges of the plate can be written as:

$$\overline{u}_2(0,\bar{x}_3) = 0, \overline{u}_2(L,\bar{x}_3) = 0, \tag{21}$$

$$M_{11}(0,\bar{x}_3) = -\overline{D}_{16}\left(\frac{\partial^2 \overline{u}_2}{\partial \bar{x}_1 \partial \bar{x}_3}\right)_{\bar{x}_1=0} - \overline{D}_{13}\left(\frac{\partial^2 \overline{u}_2}{\partial \bar{x}_3^2}\right)_{\bar{x}_1=0} - \overline{D}_{11}\left(\frac{\partial^2 \overline{u}_2}{\partial \bar{x}_1^2}\right)_{\bar{x}_1=0} = -k_r\left(\frac{\partial \overline{u}_2}{\partial \bar{x}_1}\right)_{\bar{x}_1=0}, \tag{22}$$

$$M_{11}(L,\bar{x}_3) = -\overline{D}_{16}\left(\frac{\partial^2 \overline{u}_2}{\partial \bar{x}_1 \partial \bar{x}_3}\right)_{\bar{x}_1=L} - \overline{D}_{13}\left(\frac{\partial^2 \overline{u}_2}{\partial \bar{x}_3^2}\right)_{\bar{x}_1=L} - \overline{D}_{11}\left(\frac{\partial^2 \overline{u}_2}{\partial \bar{x}_1^2}\right)_{\bar{x}_1=0} = k_r\left(\frac{\partial \overline{u}_2}{\partial \bar{x}_1}\right)_{\bar{x}_1=L} \tag{23}$$

where $\overline{D}_{ij}$ is the element of the plate bending stiffness matrix defined with respect to the ($\bar{x}_1, \bar{x}_2$, and $\bar{x}_3$) coordinate system and k_r is the stiffness of the edge rotational restraint due to unbuckled adjacent plate or plates.

Simplifying the Eqs. (22)-(23) under the assumption of cylindrical bending and with the substitution of Eq. (20), following can be obtained [26]:

$$R = \frac{1}{1 + \frac{4\pi \overline{D}_{11}}{L k_r}}. \tag{24}$$

Total potential energy of the plate can be written as sum of strain energy due to bending, strain energy stored in the rotational restraint, and the work done by the applied load:

$$\Pi = U_b + U_r + W \tag{25}$$

where;

$$U_b = \frac{1}{2}\iint \overline{D}_{11}\left(\frac{\partial^2 \overline{u}_2}{\partial \bar{x}_1^2}\right)^2 + 2\overline{D}_{13}\frac{\partial^2 \overline{u}_2}{\partial \bar{x}_1^2}\frac{\partial^2 \overline{u}_2}{\partial \bar{x}_3^2} + \overline{D}_{33}\left(\frac{\partial^2 \overline{u}_2}{\partial \bar{x}_3^2}\right)^2 + 4\overline{D}_{16}\frac{\partial^2 \overline{u}_2}{\partial \bar{x}_1^2}\frac{\partial^2 \overline{u}_2}{\partial \bar{x}_1 \partial \bar{x}_3} + 4\overline{D}_{36}\frac{\partial^2 \overline{u}_2}{\partial \bar{x}_3^2}\frac{\partial^2 \overline{u}_2}{\partial \bar{x}_1 \partial \bar{x}_3} + 4\overline{D}_{66}\left(\frac{\partial^2 \overline{u}_2}{\partial \bar{x}_1 \partial \bar{x}_3}\right)^2 d\bar{x}_1 d\bar{x}_3, \tag{26}$$

2.2. Critical shear buckling load of the composite plate

Rayliegh-Ritz method is used to calculate the critical shear buckling load of the composite plate. Consider a plate subjected to in-plane shear with rotationally restrained along the two longer edges ($b > 3L$) and simply supported along the two shorter edges (Fig. 5). The out-of-plane displacement of the plate under shear buckling may be expressed using a trigonometric function [26] as:

$$\overline{u}_2(\bar{x}_1,\bar{x}_3) = A_o\left[(1-R)sin\left(\frac{\pi \bar{x}_1}{L}\right) + R\left(1 - cos\left(\frac{2\pi \bar{x}_1}{L}\right)\right)\right] sin\left(\frac{\pi(\bar{x}_3 - \beta \bar{x}_1)}{\mu L}\right), \tag{20}$$

where $\overline{u}_2(\bar{x}_1,\bar{x}_3)$ is the out-of-plane displacement of plate-α in direction-$\bar{x}_2$, A_o, μ, and β are the amplitude of the wave, ratio of the half wave length to L, and skew angle of the wave, respectively. The function consists of a weighted term R, which takes into account the degree of rotational restraint of the plate. When R becomes zero then the

$$U_r = \frac{1}{2}\int k_r\left(\frac{\partial \overline{u}_2}{\partial \bar{x}_1}\right)^2_{\bar{x}_1=0} + k_r\left(\frac{\partial \overline{u}_2}{\partial \bar{x}_1}\right)^2_{\bar{x}_1=L} d\bar{x}_3, \tag{27}$$

$$W = \iint \overline{F}\frac{\partial \overline{u}_2}{\partial \bar{x}_1}\frac{\partial \overline{u}_2}{\partial \bar{x}_3} d\bar{x}_1 d\bar{x}_3. \tag{28}$$

Substituting the displacement function (Eq. (20)) into Eqs. (26)-(28) and then getting the first variation of total potential energy of the plate gives:

$$\delta\Pi = \delta U_b + \delta U_r + \delta W = 0 \tag{29}$$

By simplifying Eq. (29), the shear buckling load of the plate can be determined as:

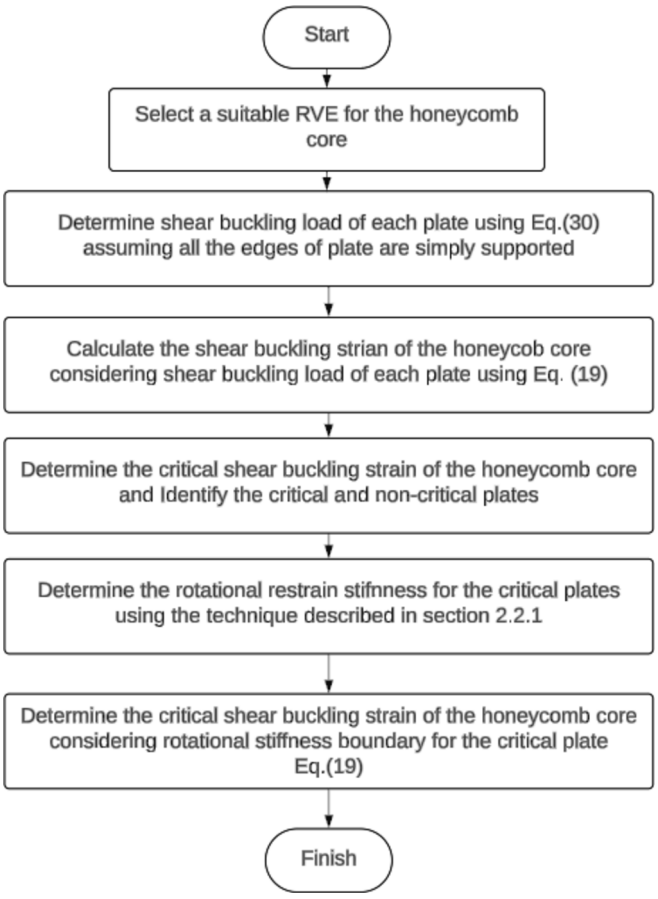

Fig. 6. Procedure for determining the critical shear buckling strain of the honeycomb core.

$$\overline{F} = \frac{\pi^2}{L^2}\left[\left(\frac{\beta^3}{2\mu^2}+\frac{\mu^2}{2\beta}+3\beta\right)\overline{D}_{11}+\frac{\overline{D}_{33}}{2\mu^2\beta}+\left(\frac{\beta}{\mu^2}+\frac{1}{\beta}\right)\overline{D}_{13}-\left(\frac{2\beta^2}{\mu^2}+\frac{6\pi^2}{L^2}\right)\overline{D}_{16}-\frac{2\overline{D}_{36}}{\mu^2}+\left(\frac{2\beta}{\mu^2}+\frac{2}{\beta}\right)\overline{D}_{66}\right]+\frac{3\pi^3R^2}{2L^2\beta(3\pi+R_n)}\left[\left(6\beta^2+26\mu^2\right)\overline{D}_{11}+2\overline{D}_{13}-12\beta\overline{D}_{16}+4\overline{D}_{66}+\frac{4k_r\mu^2L(-1+R)^2}{\pi^2R^2}\right], \tag{30}$$

where;

$$R_n = 32R - 6\pi R - 32R^2 + 12\pi R^2. \tag{31}$$

In order to find the minimum critical shear buckling load $\overline{F}_{cr}$, the Eq. (30) has to be minimised with respect to two unknowns β and μ. Here a numerical solution procedure is implemented using MATLAB 'fmincon' function to get the critical skew angle β_{cr} and critical aspect ratio μ_{cr}. The upper and lower limits for the β and μ are defined as $[0, \pi/2]$ and $[0, b/L]$ respectively for positive shear load and $[-\pi/2, 0]$ and $[0, b/L]$ respectively for the negative shear load acting on the plate. Plate will be subject to positive or negative shear depending on the applied global shear strain and the plate position in the RVE.

2.2.1. *Determination of rotational stiffness*

Depending on the shear load carried by each plate, core walls may not buckle simultaneously. Therefore, when one or more plates buckle (referred to as 'critical plate') at a time, other adjacent non-buckled plate or plates (referred to as 'restraining plate') restrain the rotation of the critical plate or plates. Therefore, the boundary of the critical plate should be considered to lie between simply supported and fixed supported for more accurate predictions. Here the effect of the rotational restraint provided by the restraining plates at boundaries of the critical plates against buckling should be considered. The critical plates and restraining plates of the RVE could be identified based on the prediction of shear buckling loads considering all edges simply supported conditions. Rotational stiffness provided by the restraining plates can be conservatively written in the following form assuming cylindrical bending [27] of the plate:

$$k_r = \frac{c(\overline{D}_{11})_{rs}}{L}\frac{1}{A_r} \tag{32}$$

where c is equal to 2 when the restraining plate is subjected to the equal

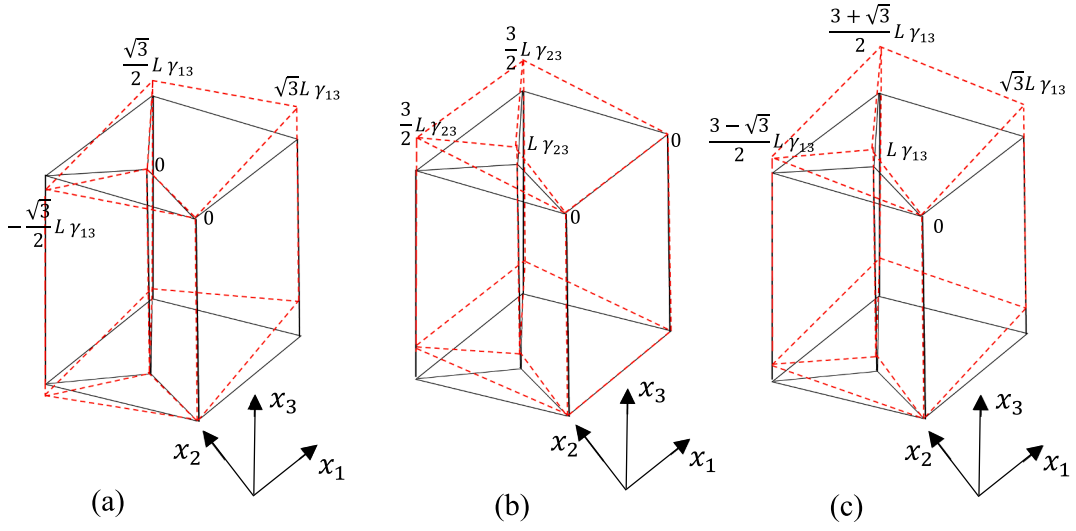

Fig. 7. Deformed configuration of RVE with identical composite plates under the shear load (a) γ_{13} (b) γ_{23} and (c).$\gamma_{13}/\gamma_{23} = 1$

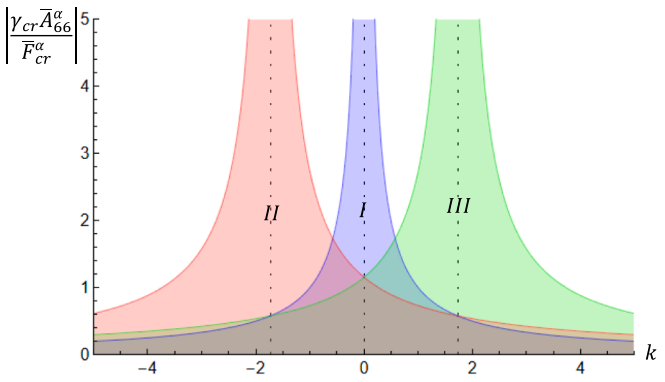

Fig. 8. Failure phase map of the honeycomb core with identical orthotropic plates.

and opposite moment and A_r is the amplification factor depending on the loading on the restraining plate. The factor A_r is defined as [27]:

$$A_r = \frac{1}{1 - \frac{(\overline{F})^{ss}_{rs}}{(\overline{F}_{cr})^{ss}_{rs}}}, \tag{33}$$

the ratio $(\overline{F})^{ss}_{rs}/(\overline{F}_{cr})^{ss}_{rs}$ being defined as follows:

$$\frac{(\overline{F})^{ss}_{rs}}{(\overline{F}_{cr})^{ss}_{rs}} = \frac{\overline{A}_{66}(\overline{\gamma})^{ss}_{rs}}{\overline{A}_{66}(\overline{\gamma}_{cr})^{ss}_{rs}} = \frac{(\overline{\gamma})^{ss}_{rs}}{(\overline{\gamma}_{cr})^{ss}_{rs}}, \tag{34}$$

where $(\overline{F}_{cr})^{ss}_{rs}$ is the critical shear buckling load of restraining plate under simply supported condition and $(\overline{F})^{ss}_{rs}$ is the shear load carried by the restraining plate at the time of buckling of the critical plate under simply supported condition. In the following it is presented two examples to illustrate the calculation of k_r:1 If plate-*II* and plate-*III* buckle simultaneously before plate-*I*, then plate-*I* will restrain the rotation of plate-*II* and plate-*III*. Rotational stiffness provided by the plate-*I* can be determined as follows:

$$k_r = \frac{1}{2}\frac{2\overline{D}^{I}_{11}}{L_1}\frac{1}{A^{I}_r}. \tag{35}$$

2 If plate-*III* only buckles first, then plate-*I* and plate-*II* together will restrain the rotation of plate-*III*. Rotational stiffness provided by the restraining plates can be determined as follows:

$$k_r = \frac{2\overline{D}^{II}_{11}}{L_2}\frac{1}{A^{II}_r} + \frac{2\overline{D}^{III}_{11}}{L_2}\frac{1}{A^{III}_r}. \tag{36}$$

Similar way, other scenarios can be considered by identifying the critical plate and restraining plates. Once the rotational stiffness of the critical plate is determined, then the critical shear buckling strain of the honeycomb core can be calculated following procedure shown in Fig. 6.

3. Theoretical analysis

3.1. Hexagonal core with identical plates

Let's consider that all the plates in the RVE (Fig. 2) have an identical fibre layer arrangement, length(L), and thickness(t). Typical deformed configurations of regular hexagonal ($\theta = 120^o$) core in Fig. 7 illustrates the nodal displacements at each plate under different global shear strain of the RVE. For the RVE subjected to shear strain γ_{13} (Fig. 7(a)), only the plate-*II* and plate-*III* carry the load, the plate-*I* does not take any shear load. Plate-*II* and plate-*III* are subject to positive shear and negative shear respectively. Since the magnitude of shear strains are equal, both plates will buckle simultaneously if the plates are fabricated with orthotropic laminate. This is not true when plates are fabricated using angle-ply laminates having bend-twist coupling. In such cases, the shear buckling loads for the plates will be different depending on the fibre orientations; therefore, only one of inclined plates (Plate-*II* or plate-*III*) will buckle first. When the RVE is subjected to shear strain γ_{23}(Fig. 7(b)), all the plates experience positive shear and plate-*I* is subjected to largest shear strain, therefore, it will buckle first because the material and geometric parameters are identical for all three plates. Similarly, when the RVE is subjected to combined shear of $\gamma_{23}/\gamma_{13} = 1$, plate-*III* will buckle first.

It can be noted that depending on applied shear strain ratio on the RVE, the critical plate and critical shear buckling strain of the core can be different which may be easily identified using a phase failure map in Fig. 8. As all plates are identical, the magnitude of the term $\overline{F}^{\alpha}_{cr}/\overline{A}^{\alpha}_{66}$ (Eq. (19)) is equal for all three plates if the plates are orthotropic laminates.

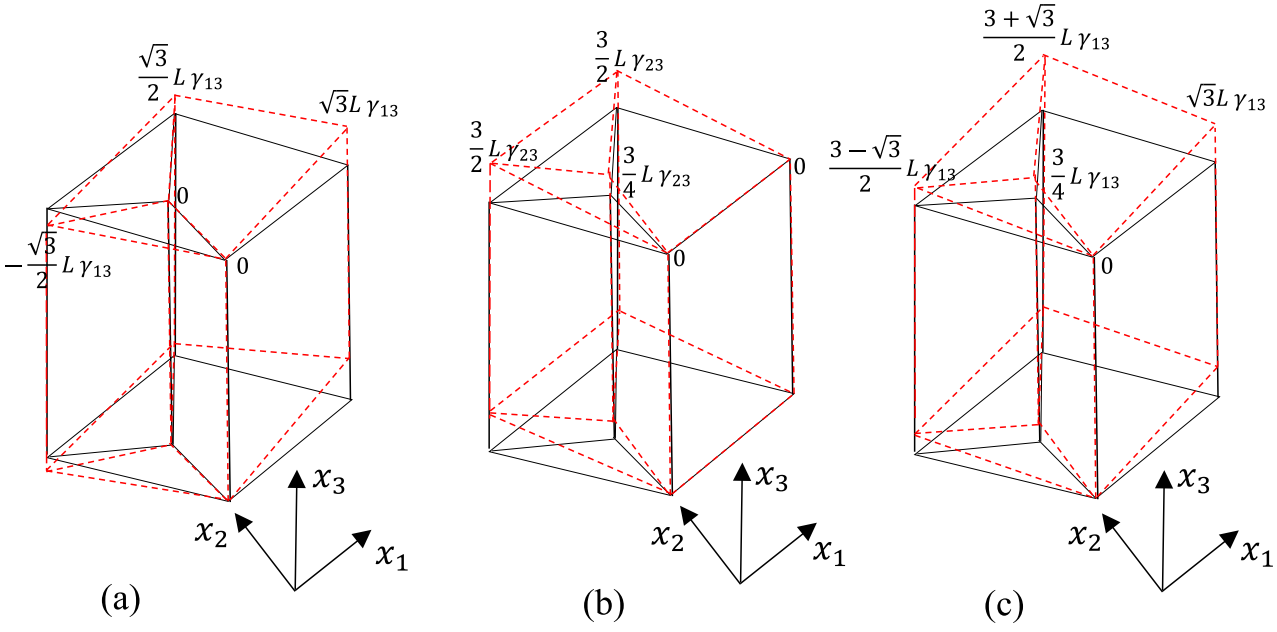

Fig. 9. Deformed configuration of RVE with non-identical composite plates under the shear load (a) γ_{13}, (b) γ_{23}, and (c)$\gamma_{13}/\gamma_{23} = 1$.

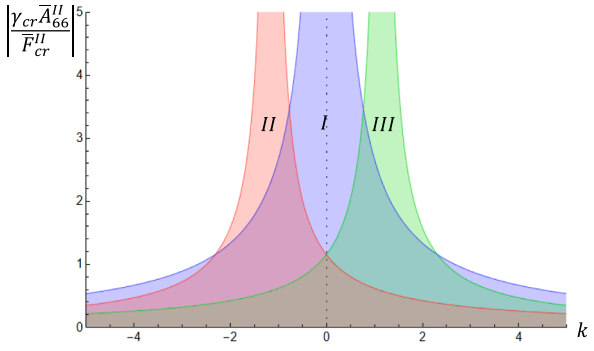

Fig. 10. Failure phase map of the hexagonal core with non-identical orthotropic plates. Plate-*I* has double thickness of plate-*II* and plate-*III*.

Then the phase failure map can be plotted based on the Eq. (37) simplified from Eq. (19):

$$\gamma_{cr} = min\left\{\left|\frac{\bar{F}^{I}_{cr}}{k\bar{A}^{I}_{66}}\right|, \left|\frac{2\bar{F}^{II}_{cr}}{\bar{A}^{II}_{66}(k-\sqrt{3})}\right|, \left|\frac{2\bar{F}^{III}_{cr}}{\bar{A}^{III}_{66}(k+\sqrt{3})}\right|\right\}. \tag{37}$$

From the phase failure map in Fig. 8, we can identify the following conditions:

- if $k > \sqrt{3}$ or $k < -\sqrt{3}$, then plate-*I* buckles first,
- if $k = 0$, then plate-*II* and plate-*III* buckle simultaneously before plate-*I* ,
- if $k = \sqrt{3}$, then plate-*I* and plate-*II* buckle simultaneously before plate-*III*,
- if $k = -\sqrt{3}$, then plate-*I* and plate-*III* buckle simultaneously before plate-*II*,
- if $0 < k < \sqrt{3}$, then only plate-*II* buckles first, and
- if $-\sqrt{3} < k < 0$, then plate-*III* buckles first.

The failure map in Fig. 8 shows a coloured region for each plate where the plate is safe against the buckling under the applied shear load. The common intersecting region of all three plates shows a feasible design region where the hexagonal core with identical plates is safe against shear buckling.

3.2. Hexagonal core with non-identical plates

If plate-*II* and plate-*III* have an identical fibre layer arrangement, length (*L*) and thickness (*t*), and plate-*I* has double thickness (*2 t*), same length and symmetric fibre layup of plate-*II* and plate-*III*, then deformed configurations of RVE of regular hexagonal ($\theta = 120^o$) core for different shear strain conditions can be plotted as in Fig. 9. The plate-*II* and plate-*III* will buckle simultaneously under both the shear strain γ_{13} and γ_{13}, however, when RVE is subjected to γ_{23}, both plates experience shear in the same direction (both positive) contrast to the γ_{13} loading (Fig. 9(a)-(b)). Like in the RVE with identical plates in section 3.2, in this case also plate-*III* buckles first under combined shear; however, the ratio of the shear strains between the plates are different. It can also be identified that the nodal points in the deform configurations are coplanar for the RVE with identical plates (Fig. 7); however, in the case where Plate-*I* is different to the Plate- *II* and Plate- *III*, deformed nodal points are not coplanar (Fig. 9(b)-(c)) which is not compatible with the face sheets of the sandwich panels. Therefore, honeycomb core with non-identical plates is subjected to bending due to skin effect of the sandwich panel, however, this effect can be considered minimal if the bending rigidity of the face sheets (typically thin face sheet) is very small compared to bending rigidity of the core (typically for thick core).

For the regular hexagonal core with non-identical plates, critical shear strain γ_{cr} for the buckling can be derived from Eq. (19) as:

$$\gamma_{cr} = min\left\{\left|\frac{2\bar{F}^{I}_{cr}}{3\bar{A}^{I}_{66}k}\right|, \left|\frac{4\bar{F}^{II}_{cr}}{\bar{A}^{II}_{66}(3k-2\sqrt{3})}\right|, \left|\frac{4\bar{F}^{III}_{cr}}{\bar{A}^{III}_{66}(3k+2\sqrt{3})}\right|\right\}. \tag{38}$$

Here, for the purpose of plotting the failure phase map (Fig. 10),

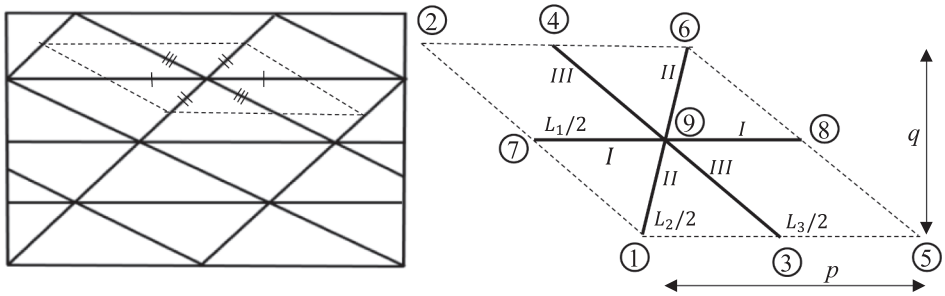

(a)

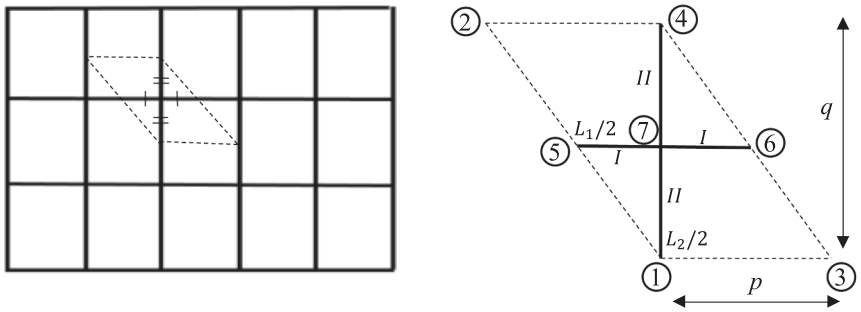

(b)

Fig. 11. RVEs of (a) triangular core (b) rectangular core.

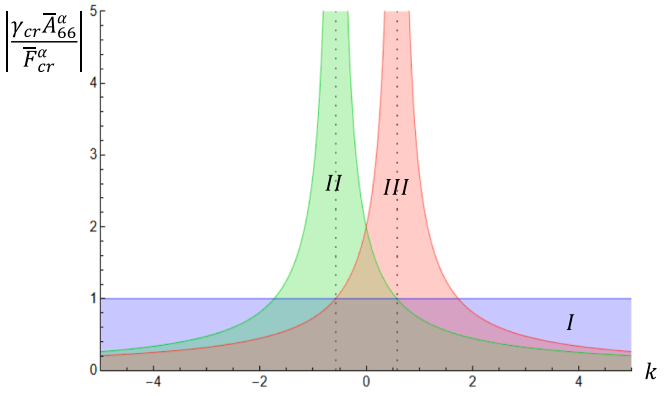

Fig. 12. Failure phase map of the triangular core with identical orthotropic plates.

additionally, we also assume that $\overline{F}^{I}_{cr} = 8\overline{F}^{II}_{cr}$. This is true when the RVE consists of plates having all the plies arranged in same orientation; however, this may or may not be true for the other fibre lay-ups of the plates. Following the condition above, the failure phase map can be used as a theoretical guidance to identify the critical plates and the critical shear strain of the hexagonal core.

4. Honeycomb core of different shapes

Following the same procedure in section 2.1, we can also derive the required equations for the critical shear strain of honeycomb core of different shapes. For rectangular and triangular cores, RVEs in Fig. 11 are used to analyse and to get the required equations for the critical shear buckling strain of the cores.

For the triangular core positive direction-$\overline{1}$ is defined for the plates-*I*, plates-*II*, and plates-*III* from 7 to 9 (or 9–8), 1 to 9 (or 9–6) and 3 to 9 (or 9–4) respectively. For the rectangular core positive direction-$\overline{x}_1$ is defined for the plates-*I* and plates-*II* from 5 to 7 (or 7–6) and 1 to 7 (or 7–4) respectively. For the triangular core in Fig. 11 with all members having identical laminate, strain at each plate can be derived as:

$$\overline{\gamma}^{I} = \gamma_{13}, \tag{39}$$

$$\overline{\gamma}^{II} = \frac{\gamma_{13}(L_1 + L_3\cos(\theta+\omega) + kL_2\sin(\omega))}{L_2}, \tag{40}$$

$$\overline{\gamma}^{III} = \frac{\gamma_{13}(L_3\cos(\theta+\omega) + kL_2\sin(\omega))}{L_3}, \tag{41}$$

where;

$$\theta = \cos^{-1}\left(\frac{\left((L_2)^2 + (L_3)^2\right) - (L_1)^2}{2L_2L_3}\right) \text{ and} \tag{42}$$

$$\omega = \cos^{-1}\left(\frac{\left((L_1)^2 + (L_2)^2\right) - (L_3)^2}{2L_1L_2}\right). \tag{43}$$

For an equilateral triangular core with identical laminates for all the plates, the critical shear strain of core γ_{cr} can be written as:

$$\gamma_{cr} = min\left\{\left|\frac{\overline{F}^{I}_{cr}}{\overline{A}^{I}_{66}}\right|, \left|\frac{2\overline{F}^{II}_{cr}}{\overline{A}^{II}_{66}\left(1+\sqrt{3k}\right)}\right|, \left|\frac{2\overline{F}^{III}_{cr}}{\overline{A}^{III}_{66}\left(-1+\sqrt{3}\right)}\right|\right\}. \tag{44}$$

The failure phase map in Fig. 11 can be plotted using Eq. (44).

From the failure phase map in Fig. 12, we can identify that:

- if $-\frac{1}{\sqrt{3}} < k < \frac{1}{\sqrt{3}}$, then the plate-*I* buckles first,
- if $k = \frac{1}{\sqrt{3}}$, then plate-*I* and plate-*II* buckle simultaneously,
- if $k = -\frac{1}{\sqrt{3}}$, then plate-*I* and plate-*III* buckle simultaneously,
- if $k > \frac{1}{\sqrt{3}}$, then plate-*II* buckles first and
- if $k < -\frac{1}{\sqrt{3}}$, then only plate-*III* buckles first.

For rectangular honeycomb core, regardless of length and stiffness ratio of the plates, we will get the relationship that applied shear strain in each direction is equal to shear strain at each plate when the plates are orthotropic laminate:

$$\overline{\gamma}^{I}_{13} = \gamma_{13}, \tag{45}$$

$$\overline{\gamma}^{II}_{13} = k\gamma_{13}. \tag{46}$$

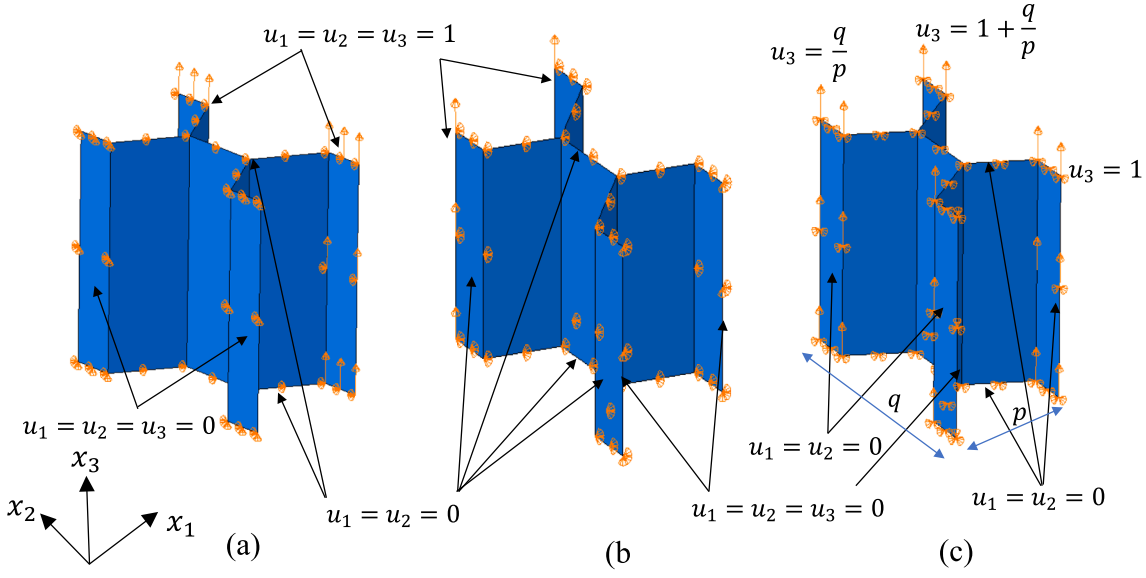

Fig. 13. FE models analysed for the shear load (a) γ_{13}, (b) γ_{23}, and (c) $\gamma_{23}/\gamma_{13} = 1$.

Table 1
Material configuration of the walls.

Fibre lay-up	Fibre orientation (^{0})
1	0/0/90/0/0
2	0/90/90/90/0
3	90/0/0/0/90
4	45/−45/0/−45/45
5	45/−45/90/−45/45
6	45/−45/45/−45/45

5. Finite element analysis

Linear buckling analysis is carried out using ABAQUS [34] software to validate the proposed semi-analytical approach for the shear buckling of the honeycomb cores. RVEs of the hexagonal cores (Fig. 13) are modelled with S4 shell elements and material properties are assigned using composite shell section feature available in the software. The fibre orientation of each lamina is defined according to positive local direction of each plate considered in this study. The element size was selected to be 0.5 mm following a mesh convergence study. Prescribed displacement boundary conditions are used to apply the shear load on the FE models of the RVEs. Shear loads are applied to represent the following average global shear strain conditions on the RVEs: a) γ_{13}, b) γ_{23} and $\gamma_{23}/\gamma_{13} = 1$ (Fig. 13). Critical shear buckling strains and the critical plates of the RVEs are determined for positive and negative shear loading considering the three different scenarios described above.

Elastic properties of E-glass/Epoxy used for composite wall honeycomb cores with respect to principal axes of the lamina in the analysis are $\overline{E}_1 = 38600\,Nmm^{-2}$, $\overline{E}_3 = 8270\,Nmm^{-2}$, $\overline{G}_{13} = 4140\,Nmm^{-2}$, $\overline{\nu}_{13} = 0.26$. Hexagonal honeycomb core wall lengths are equal and considered as $L = 50$ mm, while the depth of the core b is 150 mm. The thickness of plate-*I* of the hexagonal (Fig. 2) core is double the thickness of the inclined plates (Plates-*II* and *III*). The hexagonal cores having two different relative core density $\rho^*(1)$ of 0.072 and 0.036 are considered for the analysis. The thicknesses of plates are selected to satisfy the requirement of relative core density considered. Fibre layer sequence and orientations defined in Table 1 for the inclined plates are assigned with respect to the local axes of the plates and fibre layer sequence and orientations of the plate-*I* is assumed to be symmetrical lay-up of the inclined plates. Each ply of the laminate has an equal thickness.

Table 2
(a) Critical shear strain of the honeycomb core ($\rho^* = 0.072$) under $\gamma_{13} = \gamma$ (positive) and $\gamma_{23} = 0$.

Fibre lay-up	Critical shear buckling strain (1)			Error%		Critical plate	
	Proposed-SS(a)	Proposed-RR(b)	FE(c)	$\frac{(a-c)}{c}\%$	$\frac{(b-c)}{c}\%$	Proposed	FE
1	0.06476	0.08574	0.08375	−22.68	2.37	*II&III*	*II&III*
2	0.06226	0.08064	0.08327	−25.23	−3.16	*II&III*	*II&III*
3	0.04234	0.06087	0.06261	−32.37	−2.78	*II&III*	*II&III*
4	0.01884	0.02797	0.02746	−31.39	1.86	*III*	*III*
5	0.01867	0.02703	0.02719	−31.35	−0.60	*III*	*III*
6	0.01636	0.02388	0.02591	−36.86	−7.84	*III*	*III*

(b) Critical shear strain of the honeycomb core ($\rho^* = 0.072$) under $\gamma_{13} = \gamma$ (negative) and $\gamma_{23} = 0$.

Fibre lay-up	Critical shear buckling strain (1)			Error %		Critical plate	
	Proposed-SS(a)	Proposed-RR(b)	FE(c)	$\frac{(a-c)}{c}\%$	$\frac{(b-c)}{c}\%$	Proposed	FE
1	0.06476	0.08574	0.08375	−22.68	2.37	*II&III*	*II&III*
2	0.06226	0.08064	0.08327	−25.23	−3.16	*II&III*	*II&III*
3	0.04234	0.06087	0.06261	−32.37	−2.78	*II&III*	*II&III*
4	0.01884	0.02797	0.02746	−31.39	1.86	*III*	*III*
5	0.01867	0.02703	0.02719	−31.35	−0.60	*III*	*III*
6	0.01636	0.02388	0.02591	−36.86	−7.84	*III*	*III*

Table 3
(a) Critical shear strain of the honeycomb core ($\rho^* = 0.072$) under $\gamma_{13} = 0$ and $\gamma_{23} = \gamma$ (positive).

Fibre lay-up	Critical shear buckling strain (1)			Error %		Critical plate	
	Proposed-SS(a)	Proposed-RR(b)	FE(c)	$\frac{(a-c)}{c}\%$	$\frac{(b-c)}{c}\%$	Proposed	FE
1	0.07478	0.09513	0.09625	−22.31	−1.17	*II&III*	*II&III*
2	0.07189	0.08900	0.09541	−24.65	−6.72	*II&III*	*II&III*
3	0.04889	0.06837	0.07190	−32.00	−4.91	*II&III*	*II&III*
4	0.02175	0.02881	0.03101	−29.85	−7.08	*II&III*	*II&III*
5	0.02155	0.02802	0.03061	−29.61	−8.47	*II&III*	*II&III*
6	0.01889	0.02436	0.03066	−38.39	−20.55	*II&III*	*II&III*

b.Critical shear strain of the honeycomb core ($\rho^* = 0.072$) under $\gamma_{13} = 0$ and $\gamma_{23} = \gamma$ (negative).

Fibre lay-up	Critical shear buckling strain (1)			Error %		Critical plate	
	Proposed-SS(a)	Proposed-RR(b)	FE(c)	$\frac{(a-c)}{c}\%$	$\frac{(b-c)}{c}\%$	Proposed	FE
1	0.07478	0.09513	0.09625	−22.31	−1.17	*II&III*	*II&III*
2	0.07189	0.08900	0.09541	−24.65	−6.72	*II&III*	*II&III*
3	0.04889	0.06837	0.07190	−32.00	−4.91	*II&III*	*II&III*
4	0.03924	0.04944	0.05101	−23.08	−3.08	*II&III*	*II&III*
5	0.03900	0.04738	0.05043	−22.66	−6.04	*II&III*	*II&III*
6	0.03440	0.04247	0.03918	−12.20	8.40	*II&III*	*II&III*

Table 4

A. Critical shear strain of the honeycomb core ($\rho^* = 0.072$) under $\gamma_{13} = \gamma$ and $\gamma_{23} = \gamma$ (positive).

Fibre lay-up	Critical shear buckling strain (1)			Error %		Critical plate	
	Proposed-SS(a)	Proposed-RR(b)	FE(c)	$\frac{(a-c)}{c}\%$	$\frac{(b-c)}{c}\%$	Proposed	FE
1	0.03471	0.05036	0.04596	−23.24	9.58	*III*	*III*
2	0.03336	0.04760	0.04445	−24.94	7.10	*III*	*III*
3	0.02269	0.03512	0.03343	−32.13	5.06	*III*	*III*
4	0.01010	0.01494	0.01441	−29.92	3.67	*III*	*III*
5	0.01000	0.01445	0.01421	−29.65	1.65	*III*	*III*
6	0.00877	0.01275	0.01345	−34.81	−5.22	*III*	*III*

b. Critical shear strain of the honeycomb core ($\rho^* = 0.072$) under $\gamma_{13} = \gamma$ and $\gamma_{23} = \gamma$ (negative).

Fibre lay-up	Critical shear buckling strain (1)			Error %		Critical plate	
	Proposed-SS(a)	Proposed-RR(b)	FE(c)	$\frac{(a-c)}{c}\%$	$\frac{(b-c)}{c}\%$	Proposed	FE
1	0.03471	0.05036	0.04596	−23.24	9.58	*III*	*III*
2	0.03336	0.04760	0.04445	−24.94	7.10	*III*	*III*
3	0.02269	0.03512	0.03343	−32.13	5.06	*III*	*III*
4	0.01821	0.02579	0.02382	−23.56	8.26	*III*	*III*
5	0.01810	0.02499	0.02350	−22.97	6.35	*III*	*III*
6	0.01597	0.02225	0.01953	−18.21	13.95	*III*	*III*

Table 5

A. Critical shear strain of the honeycomb core ($\rho^* = 0.036$) under $\gamma_{13} = \gamma$ (positive) and $\gamma_{23} = 0$.

Fibre lay-up	Critical shear buckling strain (1)			Error %		Critical plate	
	Proposed-SS(a)	Proposed-RR(b)	FE(c)	$\frac{(a-c)}{c}\%$	$\frac{(b-c)}{c}\%$	Proposed	FE
1	0.01619	0.02344	0.02358	−31.34	−0.59	*II&III*	*II&III*
2	0.01557	0.02216	0.02315	−32.75	−4.29	*II&III*	*II&III*
3	0.01059	0.01592	0.01684	−37.10	−5.44	*II&III*	*II&III*
4	0.00471	0.00714	0.00741	−36.47	−3.69	*III*	*III*
5	0.00467	0.00695	0.00734	−36.41	−5.37	*III*	*III*
6	0.00409	0.00613	0.00700	−41.55	−12.40	*III*	*III*

b. Critical shear strain of the honeycomb core ($\rho^* = 0.036$) under $\gamma_{13} = \gamma$ (negative) and $\gamma_{23} = 0$.

Fibre lay-up	Critical shear buckling strain (1)			Error %		Critical plate	
	Proposed-SS(a)	Proposed-RR(b)	FE(c)	$\frac{(a-c)}{c}\%$	$\frac{(b-c)}{c}\%$	Proposed	FE
1	0.01619	0.02344	0.02358	−31.34	−0.59	*II&III*	*II&III*
2	0.01557	0.02216	0.02315	−32.75	−4.29	*II&III*	*II&III*
3	0.01059	0.01592	0.01684	−37.10	−5.44	*II&III*	*II&III*
4	0.00471	0.00714	0.00741	−36.47	−3.69	*III*	*III*
5	0.00467	0.00695	0.00734	−36.41	−5.37	*III*	*III*
6	0.00409	0.00613	0.00700	−41.55	−12.40	*III*	*III*

6. Results and discussion

6.1. Validation of the proposed approach

The proposed approach is used to predict the critical shear buckling load of the honeycomb core under the two different assumptions that all edges of plates are simply-supported (SS) and longer edges of plates are rotationally-restrained (RR). Predicted results for the hexagonal cores with different material configurations are then compared with results from the FE analysis. Tables 2-4 show the comparison of the results for the hexagonal cores with relative core density of 0.072 and Tables 5-7 show the comparisons for the relative core density of 0.036. Both positive and negative critical strains of the hexagonal cores have been calculated and compared against the FE results. For the negative critical shear strain of the hexagonal cores, the absolutes values are shown in the Tables.

It can be seen from Tables 2-7 that the predictions using the proposed approach give conservative results for all the different cases under the assumption that all the plate edges are simply-supported. The error percentage varies approximately from −12 % to −42 %, considering two different core densities. On the other hand, except for a few cases of fibre lay-up 6, the predictions are much closer to FE results, assuming that longer edges of the plates are rotationally-restrained. The fibre lay-up 6 creates extensional-shear and bend-twist coupling within the plate. Although the proposed analytical solution in Eq. (30) accounts for bend-twist coupling, the extensional-shear coupling is not considered. Strong extensional-shrear coupling therefore leads to either underestimate or overestimate the critical strain depending on the normal stress caused due to the coupling is tensile or compressive respectively. In all other fibre lay-ups, the absolute error is less than 10 % (Table 2-7) for all the different load cases and for the different core densities. Under the shear loading of γ_{13}, we get the same absolute values of critical shear strains regardless positive and negative direction of applied shear load on the RVE for all the different material configurations (Tables 2 and 5). Under this shear loading on the RVE, only inclined plates (Plate-*II* and Plate-*III*) carry the shear load, and one of the inclined plates is under positive shear and other is under negative shear (Fig. 14(a)-(d)). For the RVE with cross-ply laminates (material lay-up 1–3 in Table 1), both the inclined plates buckle simultaneously since the magnitude of critical shear strains are equal. However, for the RVE having angle-ply laminates (fibre lay-ups 4–6 in Table 1), the magnitude of critical shear strains is different in the inclined plates due to the effect of bend-twist coupling of

Table 6

A. Critical shear strain of the honeycomb core ($\rho^* = 0.036$) under $\gamma_{13} = 0$ and $\gamma_{23} = \gamma$ (positive).

Fibre lay-up	Critical shear buckling strain (1)			Error %		Critical plate	
	Proposed-SS(a)	Proposed-RR(b)	FE(c)	$\frac{(a-c)}{c}\%$	$\frac{(b-c)}{c}\%$	Proposed	FE
1	0.01870	0.02578	0.02709	−30.96	−4.82	*II&III*	*II&III*
2	0.01797	0.02425	0.02652	−32.24	−8.56	*II&III*	*II&III*
3	0.01222	0.01809	0.01934	−36.81	−6.46	*II&III*	*II&III*
4	0.00588	0.00806	0.00835	−29.61	−3.51	*II&III*	*II&III*
5	0.00583	0.00777	0.00825	−29.36	−5.86	*II&III*	*II&III*
6	0.00505	0.00679	0.00827	−38.96	−17.93	*II&III*	*II&III*

b.Critical shear strain of the honeycomb core ($\rho^* = 0.036$) under $\gamma_{13} = 0$ and $\gamma_{23} = \gamma$ (negative).

Fibre lay-up	Critical shear buckling strain (1)			Error %		Critical plate	
	Proposed-SS(a)	Proposed-RR(b)	FE(c)	$\frac{(a-c)}{c}\%$	$\frac{(b-c)}{c}\%$	Proposed	FE
1	0.01870	0.02578	0.02709	−30.96	−4.82	*II&III*	*II&III*
2	0.01797	0.02425	0.02652	−32.24	−8.56	*II&III*	*II&III*
3	0.01222	0.01809	0.01934	−36.81	−6.46	*II&III*	*II&III*
4	0.01061	0.01373	0.01407	−24.61	−2.44	*II&III*	*II&III*
5	0.01055	0.01326	0.01391	−24.17	−4.70	*II&III*	*II&III*
6	0.00860	0.01062	0.01076	−20.07	−1.30	*II&III*	*II&III*

Table 7

A. Critical shear strain of the honeycomb core ($\rho^* = 0.036$) under $\gamma_{13} = \gamma$ and $\gamma_{23} = \gamma$ (positive).

Fibre lay-up	Critical shear buckling strain (1)			Error %		Critical plate	
	Proposed-SS(a)	Proposed-RR(b)	FE(c)	$\frac{(a-c)}{c}\%$	$\frac{(b-c)}{c}\%$	Proposed	FE
1	0.00868	0.01259	0.01255	−30.85	0.30	*III*	*III*
2	0.00834	0.01190	0.01225	−31.93	−2.87	*III*	*III*
3	0.00567	0.00878	0.00889	−36.23	−1.25	*III*	*III*
4	0.00252	0.00374	0.00386	−34.66	−3.03	*III*	*III*
5	0.00250	0.00361	0.00381	−34.39	−5.26	*III*	*III*
6	0.00219	0.00319	0.00361	−39.41	−11.74	*III*	*III*

b. Critical shear strain of the honeycomb core ($\rho^* = 0.036$) under $\gamma_{13} = \gamma$ and $\gamma_{23} = \gamma$ (negative).

Fibre lay-up	Critical shear buckling strain (1)			Error %		Critical plate	
	Proposed-SS(a)	Proposed-RR(b)	FE(c)	$\frac{(a-c)}{c}\%$	$\frac{(b-c)}{c}\%$	Proposed	FE
1	0.00868	0.01259	0.01255	−30.85	0.30	*III*	*III*
2	0.00834	0.01190	0.01225	−31.93	−2.87	*III*	*III*
3	0.00567	0.00878	0.00889	−36.23	−1.25	*III*	*III*
4	0.00455	0.00645	0.00656	−30.63	−1.66	*III*	*III*
5	0.00453	0.00625	0.00649	−30.20	−3.69	*III*	*III*
6	0.00399	0.00556	0.00538	−25.85	3.33	*III*	*III*

the laminate; therefore, only one of inclined plates which has the lowest critical shear buckling load buckles. When the direction of the shear load on the RVE changes other inclined plate buckles at the same absolute critical strain. Therefore, the change in the direction (positive to negative or vice-versa) of the applied loading does not change the critical shear buckling strain of the hexagonal core under γ_{13}.

Under shear loading of γ_{23} on the RVE, critical shear buckling strain of the hexagonal core changes depending on the positive and negative direction of the applied shear load (Tables 3 and 6). Under γ_{23} loading, for all the material configurations and for both negative shear and positive shear loading, plates *II* and *III* buckle simultaneously (Fig. 14 (e)-(h)), and all the plates experience the strain in the same direction. Therefore, the change in direction of applied shear load (positive to negative or vice-versa) on the RVE gives different critical strains for the RVE having the angle-ply laminates due to the effect of bend-twist coupling. However, for the hexagonal cores with cross-ply laminates, magnitudes of the critical strains are equal regardless of positive and negative direction of loading γ_{23} on the RVE. The difference between the critical shear strains for the positive and negative shear loading γ_{23} on the RVE with the angle-ply laminates is significant (critical strain for negative shear approximately 1.7 times critical strain for the positive shear); thus, neglecting the effect of bend-twist coupling under γ_{23} loading will under or overestimate the critical shear buckling load.

Comparing the critical shear strains of the hexagonal core under shear loadings γ_{13} and γ_{23}, a slightly higher results are obtained for the shear load γ_{23} for all the fibre lay-ups in positive shear and for the cross-ply laminates in negative shear (Table 3). However, the critical strains of the hexagonal core under negative γ_{23} loading are significantly higher than for negative γ_{13} loading for the angle-ply laminates (Table 3). In the combined shear loading where γ_{13} and γ_{23} are equal, the buckling behaviour is similar to γ_{23} loading in terms of the impact of the positive and negative shear loading on the hexagonal core. However, here only one of the inclined plates (Plate-*III*) buckles (Fig. 14 (i) – (l)).

In Fig. 15, the effect of the core walls aspect ratio on the shear buckling strain of the hexagonal core under positive shear loads γ_{13} and γ_{23} is illustrated. For the honeycomb core with relatively longer plates considered in this study, the shear buckling strain approached a constant value and the proposed approach, which incorporates rotationally restrained boundaries, provides a very good agreement with FE predictions. This suggests that the proposed approach accurately captures the shear buckling of composite honeycomb cores, particularly for those having the walls with the higher aspect ratios, validating its

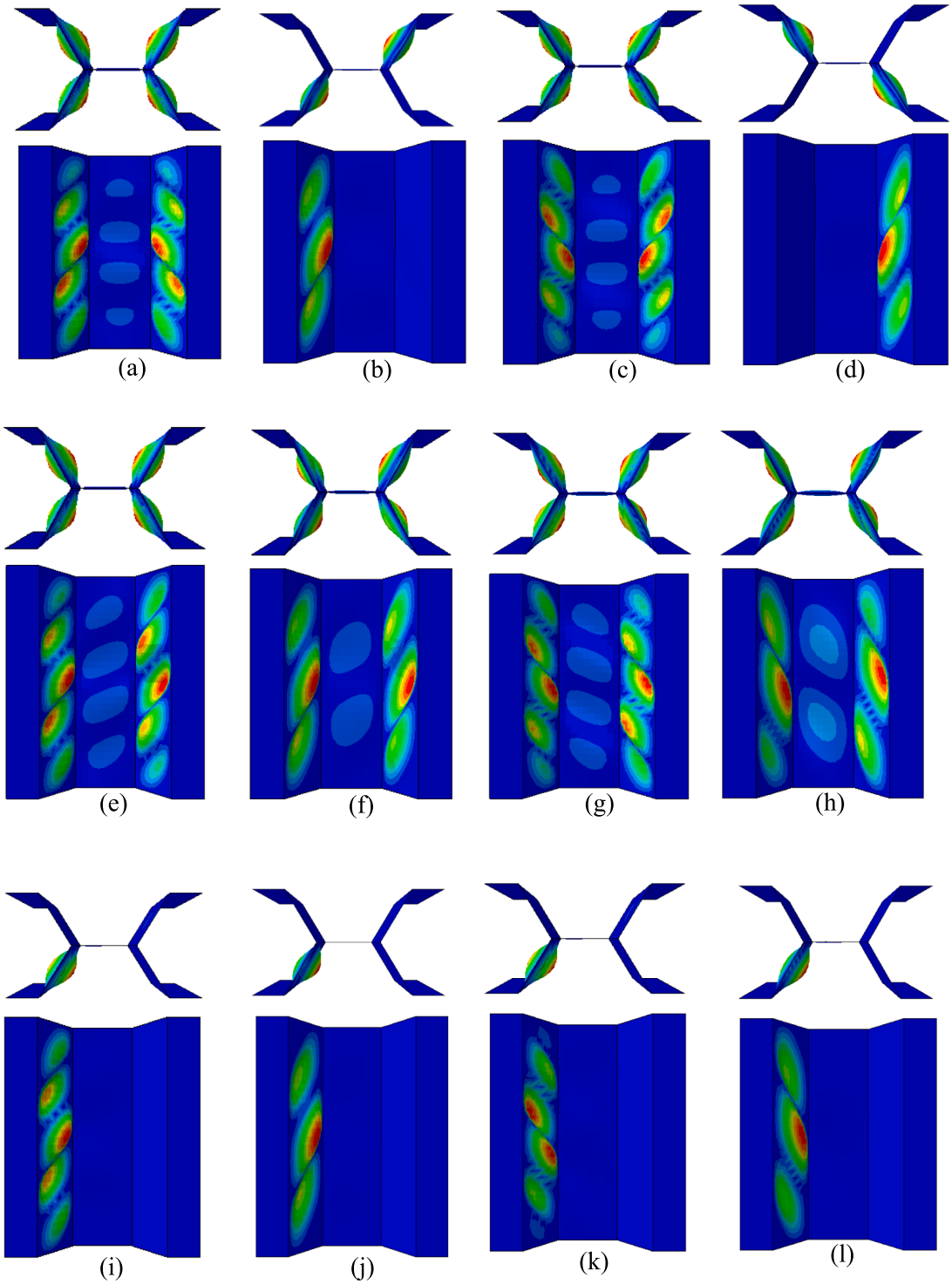

Fig. 14. Top view and side view of critical buckling mode shape for the shear load (a-b) γ_{13}(positive shear), (c-d) γ_{13}(negative shear), (e-f) γ_{23}(positive shear), (g-h) γ_{23}(negative shear), (i-j) $\gamma_{13}/\gamma_{23} = 1$(positive shear), and (k-l) $\gamma_{13}/\gamma_{23} = 1$(negative shear). The critical buckling mode shapes are shown for the hexagonal core RVEs with (0/0/90/0/0) and (45/-45/0/-45/45) laminates and relative core density of 0.072. 1st and 3rd critical mode shapes of each row are for (0/0/90/0/0) laminate and 2nd and 4th are for (45/-45/0/-45/45) laminate.

applicability and reliability in predicting the core wall buckling behaviour under shear loading.

6.2. *Influence of important parameters*

In the previous section, the predictions using the proposed approach were validated using the results from FE. In this section, the proposed approach is used to study the influence of important parameters on the critical shear buckling strain of the honeycomb core.

Fig. 16 shows the variation of the critical strains against the length ratio of the honeycomb core with the constant relative core density of 0.072. The length of plate-*II* and plate-*III* are changed while the length of plate-*I* still remains at 50 mm. The requirement of constant core density is maintained by selecting the suitable thickness for plates. All other

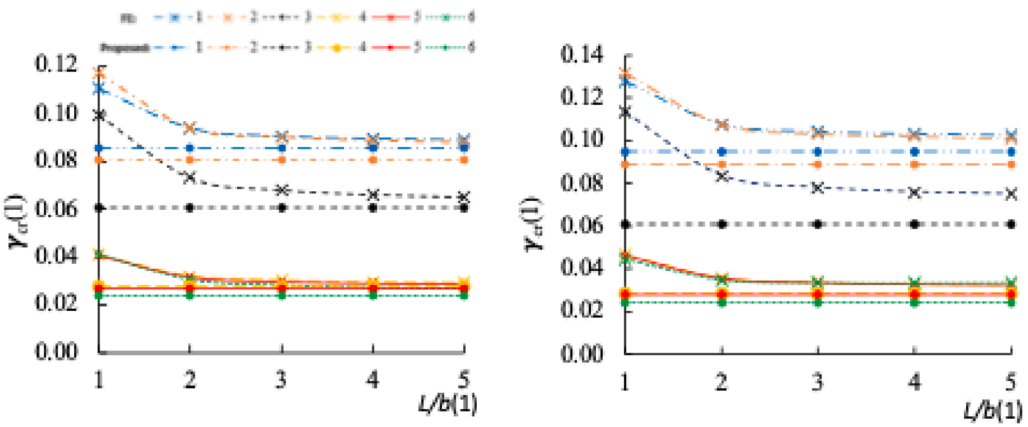

Fig. 15. Effect of the aspect ratio of core walls on the critical shear buckling strain under (a) γ_{13}(positive shear), (b) γ_{23}(positive shear).

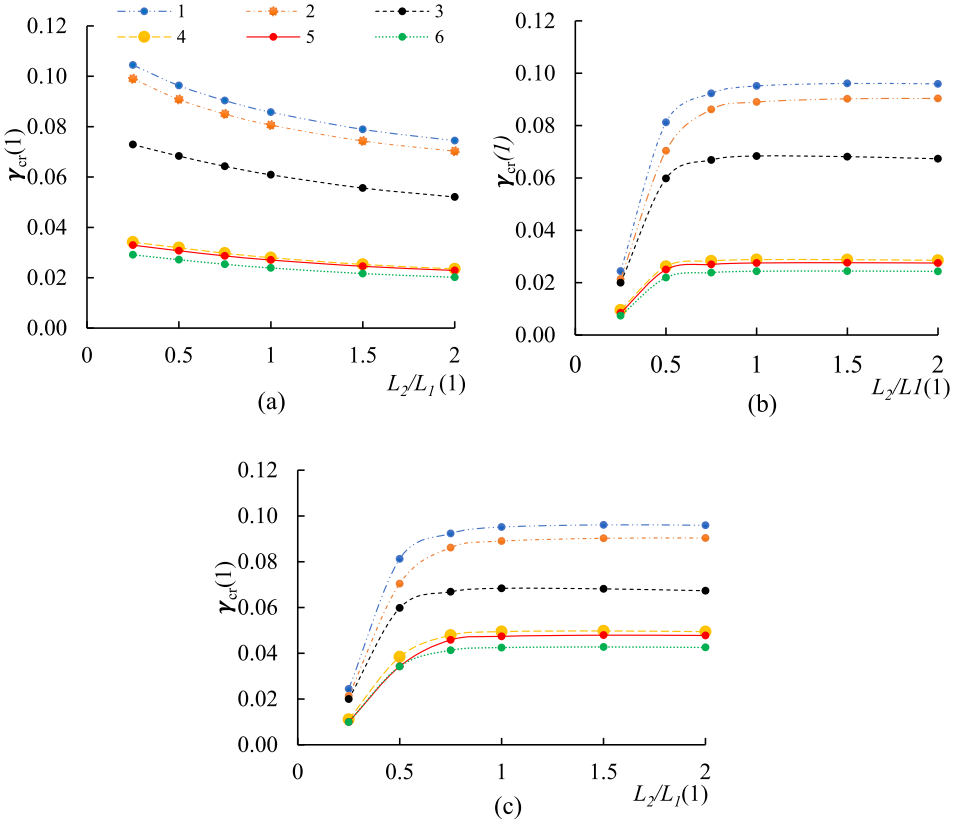

Fig. 16. Variation of the critical shear buckling strain with different length ratio between plate-II and I for the shear load (a) γ_{13} (positive and negative shear), (b) γ_{23}(positive shear) and (c) γ_{23}(negative shear).

conditions, such as the thickness ratio of plates and fibre lay-ups remain same as before. Fig. 16(a) shows the variation of the critical strain under γ_{13} shear loading. With the increase in the length ratio (L_2/L_1) of plates, the critical shear buckling strain of the hexagonal core reduces continuously. It can be understood that increasing the length of the plate-*II* and plate-*III* under constant core density reduces the thickness of the inclined plates, leading to the continuous reduction of the shear buckling load of the hexagonal core as the plate-*I* does not contribute to any load sharing due to its orientation.

On the other hand, we see different trends in the variations of the critical strains under the γ_{23} loading (Fig. 16(b)-(c)). Under γ_{23} loading, shear load on the hexagonal core is carried by all three plates; therefore, the change in the length ratio (L_2/L_1) leads to a transition of critical strain dependency of the hexagonal core between the plate-*I* and the inclined plates. At the lower length ratio, the plate-*I* buckles first and governs the critical strain of the hexagonal core. As the length ratio increases, both inclined plates buckle before the plate-*I*, and the critical strain is almost constant with the variation of the length ratio. For the cross-ply laminates, the transition of critical buckling dependency from the plate-*I* to inclined plates happens at the length ratio of 0.75 for both positive and negative shear on the RVE. For the angle ply-laminates, the transition happens at the length ratio of 0.5 for the positive shear and 0.75 for the negative shear.

Fig. 17 shows the variation of the critical strain with change of angle between the plates. The relative core density remains constant at 0.072 by changing the thickness of the plates accordingly. The maximum critical shear strains of the honeycomb are obtained at around 130° and 110° for the shear load γ_{13} and γ_{23} respectively, regardless of positive or

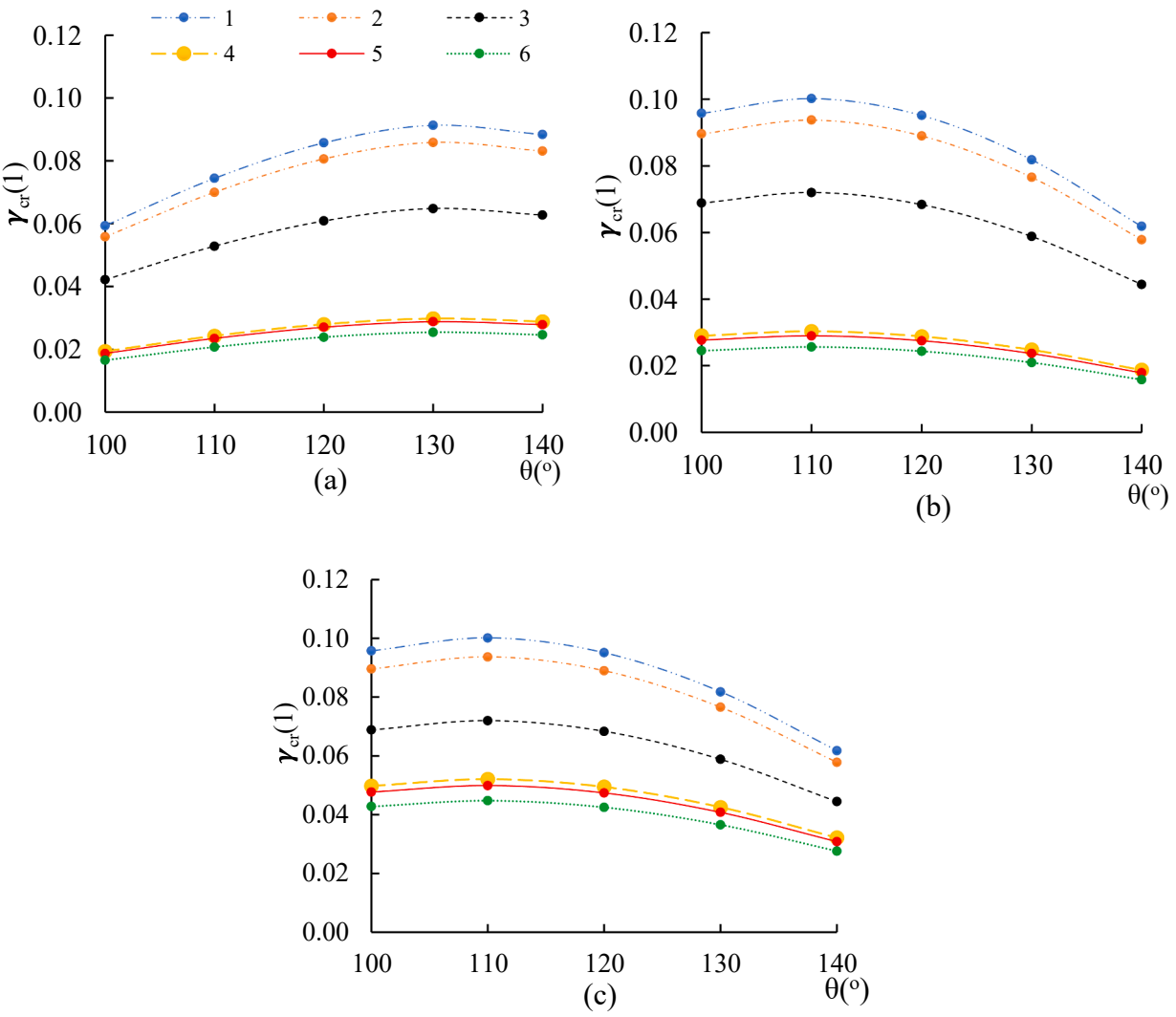

Fig. 17. Variation of the critical shear buckling strain with the angle θ between the plates for the shear load (a) γ_{13}(positive and negative shear), (b) γ_{23} (positive shear) and (c) γ_{13} (negative shear).

negative shear and the material configuration of the plates. It can be noted that the thickness of each plate at these angles is lower than plates of the regular hexagonal core (120°); however, the ratios in Eq. (19) become maximum at 130° and 110° for the respective shear loading.

Fig. 18 shows the variation of the critical strain and shear buckling strength of the hexagonal core with relative core density. The shear buckling strength of the hexagonal core is calculated by multiplying the critical strain with the effective shear stiffness [35,36] of the hexagonal core. The relative core density is varied by changing the thicknesses of the plates while keeping the length of each wall constant (50 mm); however, it can be deduced from the Eq. (19) that even if we change the length of plates (without changing the thickness) to vary the relative core density, we will get same effect on the critical shear strain as long as length ratio of the plates remains constant and the core depth to length ratio is adequate to consider as

long plate for the buckling. The Fig. 18(a)-(b) show the critical shear buckling strain and corresponding shear buckling strength for the positive and negative shear loading γ_{13}. Although the effective stiffnesses of the hexagonal cores with angle-ply laminates are higher than the effective stiffnesses of the hexagonal cores with cross-ply laminates (Fig. 18(g)-(h)), the buckling strength of the honeycomb core with cross-ply laminates are higher than angle-ply laminates for the positive and negative shear load γ_{13} (Fig. 18(b)) and positive shear load γ_{23} (Fig. 18 (d)). For the negative shear load of γ_{23}, the hexagonal cores with angle-ply laminates shows higher shear buckling strength than the cross-ply laminates (Fig. 18(f)). It can be seen from Fig. 18(a)-(f) that the shear buckling strength for the γ_{13} loading is always lower than the shear buckling strength for γ_{23} loading; therefore, for the uniaxial bending, it is always efficient to orient the plate-*I* along the longitudinal axis of the beam and to use angle-ply laminates considering the direction of the shear. However, for the plates subjected to combined shear, using the angle-ply laminates for the core is beneficial if the design is governed by the stiffness (e.g. deflection), but if it is strength governed then material configurations and geometry of the honeycomb need to be designed for the specific loadings for optimal performance.

As discussed earlier, the presence of bend-twist coupling in the angle-ply laminates positively and negatively influences the shear buckling strength of the honeycomb core. Fig. 19 shows comparisons of the critical shear buckling strains obtained without considering the bend-twist coupling (orthotropic solution $\overline{D}_{16} = 0$ and $\overline{D}_{36} = 0$) with the predictions considering the effect of bend-twist coupling for hexagonal core with fibre lay-up (45/-45/0/-45/45) in Table 1. The ratio of $\overline{D}_{16}/\overline{D}_{66}$ is varied by changing the ratio of thickness of 45/-45 plies to 0-angle plies while the laminate remains still symmetric and balanced, and the relative core density of hexagonal core is 0.072. For the γ_{13} loading, the critical strain is overestimated with orthotropic buckling solution (Fig. 19(a)). Maximum error of around 60 % (Fig. 19(b)) is occurred when the thickness of the 0-angle ply approaches zero. On the other

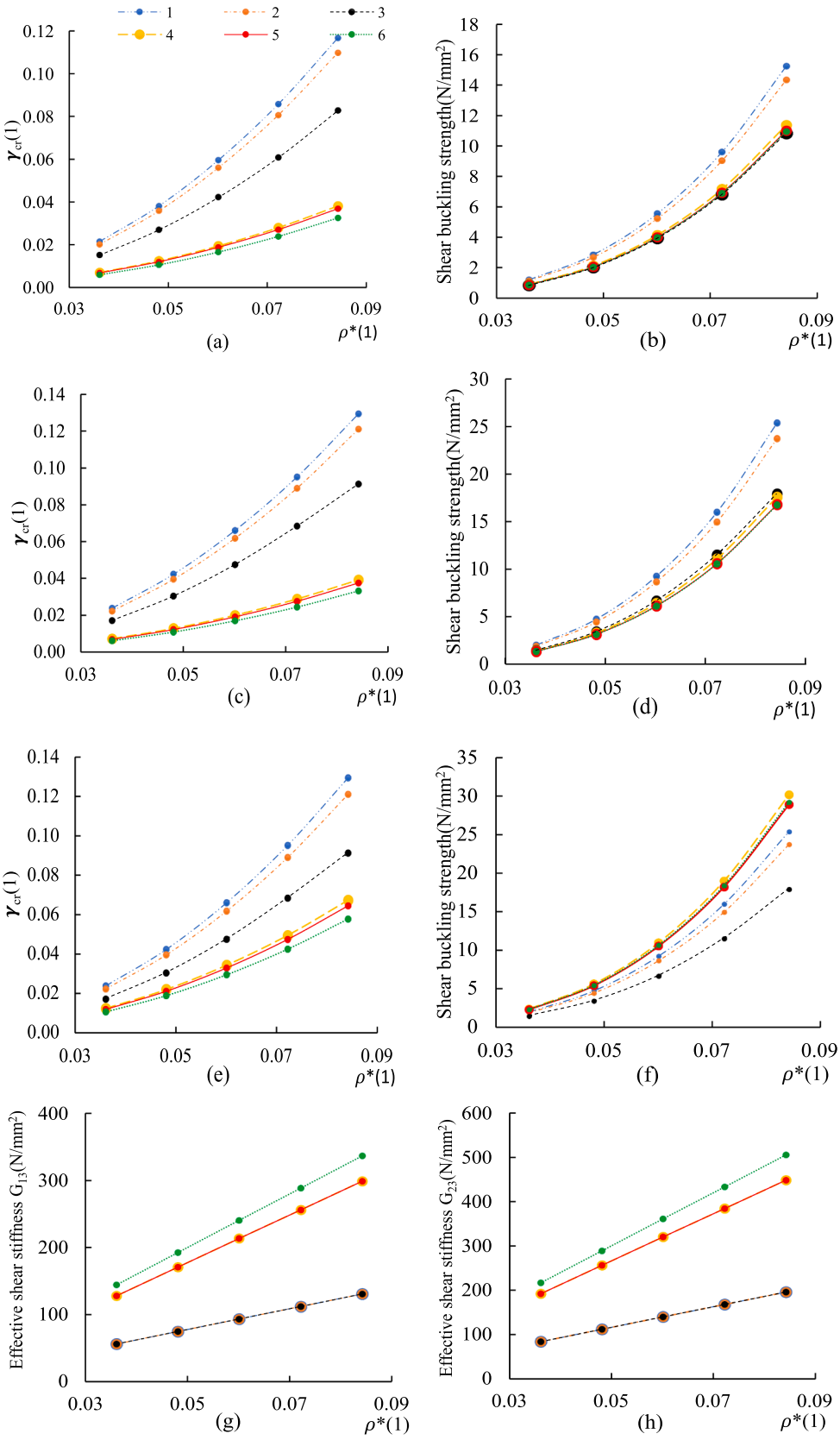

Fig. 18. Variation of the critical shear buckling strain and shear buckling strength for the shear load (a-b) γ_{13} (positive and negative shear), (c-d) γ_{23} (positive shear) and (e-f) γ_{13} (negative shear) and variation of the effective shear stiffness (g) G_{13} and (h) G_{23} with the relative core density of the hexagonal core. Shear buckling strength of the hexagonal core is calculated by multiplying the critical strain by the effective shear stiffness of the core.

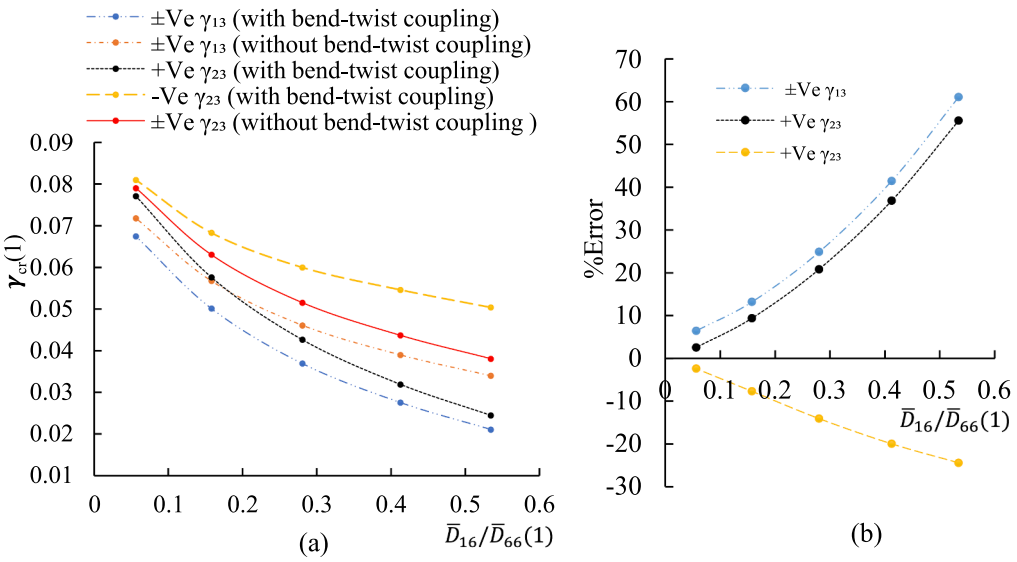

Fig. 19. (a) Comparison of the predictions of the critical shear strains with and without the consideration of bend-twist coupling for different shear loads and (b) percentage of difference in predictions between with and without bend-twist coupling. Thickness of (45/-45) plies and 0-ply of angle ply laminate (45/-45/0/-45/45) in Table 1 were varied without changing the total thickness of the laminate (constant relative core density) to vary the influence of bend-twist coupling.

hand, predictions with and without the bend-twist coupling converge to the same results as the percentage of + 45/-45 plies approaches zero. For the γ_{23} loading, the critical shear strain of the hexagonal core is overestimated by a maximum of 56 % and underestimated by 25 % for the positive and negative shear, respectively. When the thicknesses of each ply of laminate are equal (hexagonal cores considered in Tables 2–3), the error percentages are 41 %, 36 % and −20 % for positive and negative γ_{13}, positive γ_{23} and negative γ_{23}, respectively.

6.3. Comparisons between different core shapes

Fig. 20 compares critical shear buckling strains of different core shapes with an equal relative core density of 0.072. Here, the plates' lengths of equilateral triangular core and rectangular core are selected such that the characteristics dimensions p (86.6 mm) and q (75 mm) are equal to the hexagonal core considered in this study. The hexagonal core has the highest critical buckling strains for all the different load cases compared to triangular and rectangular cores (Fig. 20(a)-(f)). The superior performance of the hexagonal core compared to other core shapes is mainly due to its geometric configuration and shear loading conditions. However, under the combined shear condition, the relative reduction in the shear buckling capacity of the hexagonal core is higher than other core shapes. It can be noted that for the same relative core density and for selected plate lengths, rectangular and triangular cores have lower plate thickness than the honeycomb core. By selecting larger plate lengths for the triangular and rectangular cores, one may consider higher thickness for plates to keep the core density constant. However, it can be deduced from Eq. (19) that the critical strain of the sufficiently thick core does not vary with the length of the plate as long as the core density and length ratio between the plates remain constant.

7. Conclusions

In this study, we present a novel and accessible semi-analytical approach for predicting the critical shear buckling load of composite honeycomb cores in sandwich panels. Our proposed model exhibits a broad applicability, accommodating various honeycomb core shapes and material configurations. Notably, employing simply-supported boundary conditions for all honeycomb core edges yields conservative predictions, while rotationally restraining two longer edges aligns closely with finite element (FE) results. Analysing hexagonal honeycomb cores with cross-ply and angle-ply laminates, we unveil the consistent critical shear buckling strains of cross-ply laminates and the directional influence of angle-ply laminates due to bend-twist coupling. The study underscores the superior shear buckling performance of hexagonal cores and emphasizes the potential for optimization by adjusting both material configurations and geometric parameters. Key contributions and impacts of the paper include:

General Applicability: The proposed approach is versatile, offering predictions for various honeycomb core shapes and material configurations, showcasing its broad applicability.
Boundary Conditions Influence: By exploring different boundary conditions, the study reveals that rotationally restraining two longer edges provides predictions closely aligned with finite element (FE) results, offering a more accurate representation of critical shear buckling strains.
Material Configuration Impact: The investigation of hexagonal honeycomb cores with cross-ply and angle-ply laminates highlights the influence of material configurations on critical shear buckling loads. Notably, angle-ply laminates exhibit directional sensitivity due to bend-twist coupling effects.
Conservative vs. Accurate Predictions: The proposed model's use of simply-supported boundary conditions leads to conservative predictions, while rotationally restraining longer edges provides more accurate results, balancing efficiency and precision.
Geometric Optimization: The study emphasizes the potential for optimizing shear buckling strength not only through material configurations but also by adjusting geometric parameters of the honeycomb core.

Our approach, notable for its ease of implementation and computational efficiency compared to finite element methods, proves to be a valuable tool for optimizing honeycomb core shapes and material configurations in sandwich panel design. Beyond enhancing the understanding of shear buckling behaviour, it provides practical insights for industries focused on lightweight, high-performance structures.

While the proposed analytical approach provde many advantages as highlighted above, it is with several limitations owing to the simplifying assumptions made to make an analytical model possible. The proposed method does not account for possible extensional-shear coupling effects of the laminates. As a result, predictions may not be accurate when

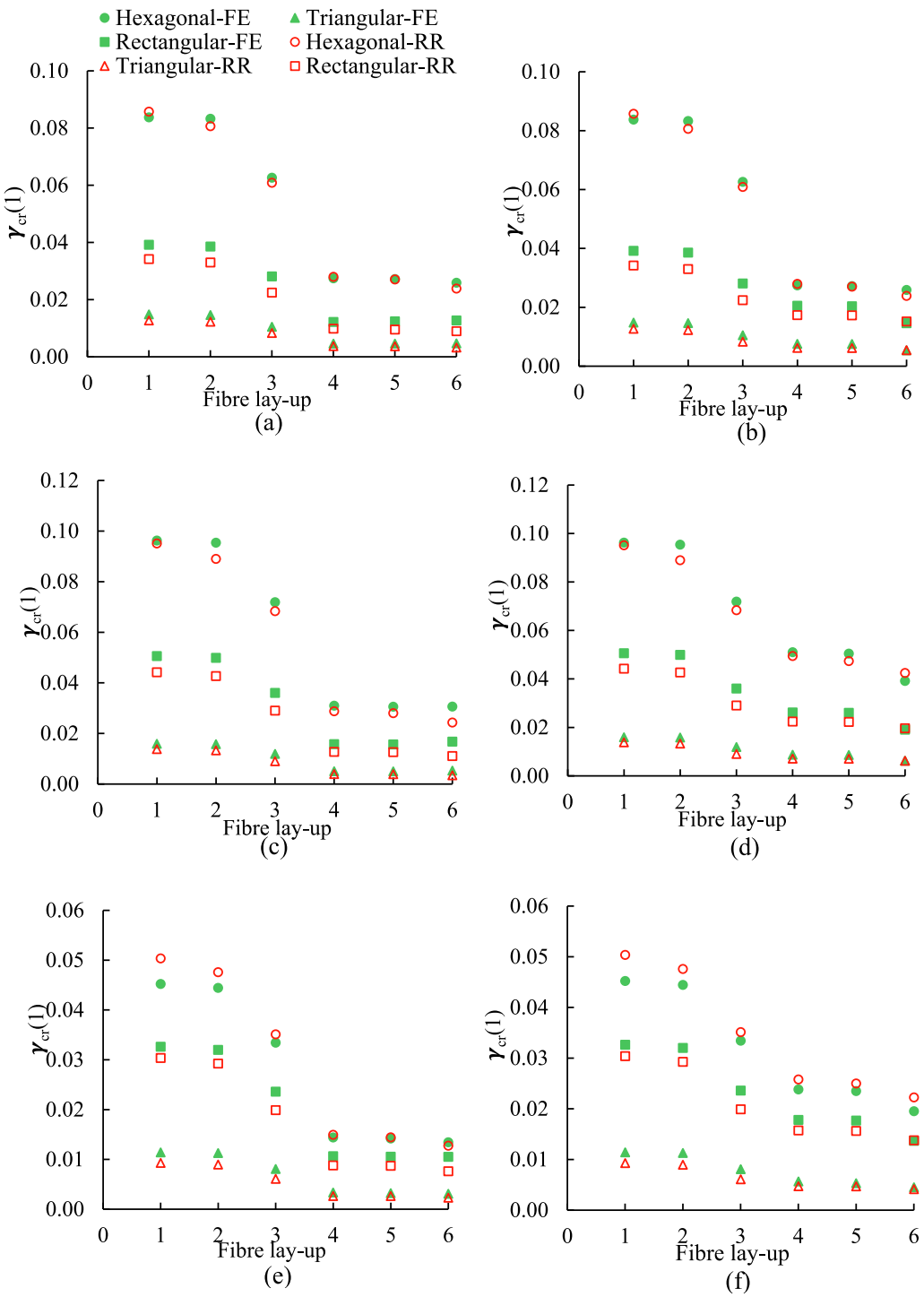

Fig. 20. Comparison of critical shear strain between cellular cores with different shapes for the shear load (a) γ_{13}(positive shear), (b) γ_{13} (negative shear), (c) γ_{23} (positive shear), (d) γ_{23} (negative shear), (e) $\gamma_{13}/\gamma_{23} = 1$ (positive shear) and (f) $\gamma_{13}/\gamma_{23} = 1$ (negative shear).

laminates with strong extensional-shear coupling are used for the honeycomb walls. The proposed solution also ignored the portantial interactions between the core and face sheets. While ignoring such effects means proposed solution is lukely to provide conservative results, this may cause potential errors interms of determining the optimal solution. In addition, analytical model assumed ideal geometric conditions and ignored the effects of imperfections. Imperfections may influence the shear buckling capacity, thus predictions may not be accurate when there are large imperfections in the core walls.

CRediT authorship contribution statement

Jasotharan Sriharan: Conceptualization, Data curation, Formal analysis, Investigation, Methodology, Visualization, Writing – original draft. **Marcelo Dias:** Writing – review & editing, Supervision, Investigation, Formal analysis, Data curation. **Sondipon Adhikari:** Writing – review & editing, Supervision, Formal analysis. **Dilum Fernando:** Writing – review & editing, Validation, Supervision, Project administration, Funding acquisition, Formal analysis, Conceptualization.

Declaration of competing interest

The authors declare that they have no known competing financial interests or personal relationships that could have appeared to influence the work reported in this paper.

Data availability

Data will be made available on request.

References

[1] Kee Paik J, Thayamballi AK, Sung KG. The strength characteristics of aluminum honeycomb sandwich panels. Thin-Walled Struct 1999;35:205–31.
[2] Wang J, Shi C, Yang N, Sun H, Liu Y, Song B. Strength, stiffness, and panel peeling strength of carbon fiber-reinforced composite sandwich structures with aluminum honeycomb cores for vehicle body. Compos Struct 2018;184:1189–96.
[3] Wei X, Xiong J, Wang J, Xu W. New advances in fiber-reinforced composite honeycomb materials. Sci China Technol Sci 2020;63:1348–70.
[4] Pehlivan L, Baykasoğlu C. An experimental study on the compressive response of CFRP honeycombs with various cell configurations. Composites B 2019;162:653–61.
[5] Vitale P, Francucci G, Rapp H, Stocchi A. Manufacturing and compressive response of ultra-lightweight CFRP cores. Compos Struct 2018;194:188–98.
[6] Petras A, Sutcliffe MPF. Failure mode maps for honeycomb sandwich panels. Compos Struct 1999;44:237–52.
[7] Wei X, Wu Q, Gao Y, Xiong J. Bending characteristics of all-composite hexagon honeycomb sandwich beams: experimental tests and a three-dimensional failure mechanism map. Mech Mater 2020;148:103401.
[8] Noor AK, Burton WS, Bert CW. Computational models for sandwich panels and shells. Appl Mech Rev 1996;49:155–99.
[9] Kapania RK, Soliman HE, Vasudeva S, Hughes O, Makhecha DP. Static analysis of sandwich panels with square Honeycomb Core. AIAA J 2008;46:627–34.
[10] Kreja I. A literature review on computational models for laminated composite and sandwich panels. Cent Eur J Eng 2011;1:59–80.
[11] Rodriguez-Ramirez JD, Castanie B, Bouvet C. Experimental and numerical analysis of the shear nonlinear behaviour of Nomex honeycomb core: Application to insert sizing. Compos Struct 2018;193:121–39.
[12] Battley MA, Stone SJ, Allen TD. The effect of thickness on the transverse shear strength of nomex honeycomb cores. J Sandw Struct Mater 2023;25:180–98.
[13] Pan S-D, Wu L-Z, Sun Y-G, Zhou Z-G, Qu J-L. Longitudinal shear strength and failure process of honeycomb cores. Compos Struct 2006;72:42–6.
[14] Zhang J, Ashby MF. The out-of-plane properties of honeycombs. Int J Mech Sci 1992;34:475–89.
[15] Pan S-D, Wu L-Z, Sun Y-G. Transverse shear modulus and strength of honeycomb cores. Compos Struct 2008;84:369–74.
[16] Banerjee S, Battley M, Bhattacharyya D. Shear strength optimization of reinforced honeycomb core materials. Mech Adv Mater Struct 2010;17:542–52.
[17] Shi G, Tong P. Local buckling of honeycomb sandwich plates under action of transverse shear forces. AIAA J 1994;32:1520–4.
[18] Cote F, Deshpande V, Fleck N. The shear response of metallic square honeycombs. J Mech Mater Struct 2006;1:1281–99.
[19] Kim B, Christensen RM. Basic two-dimensional core types for sandwich structures. Int J Mech Sci 2000;42:657–76.
[20] López Jiménez F, Triantafyllidis N. Buckling of rectangular and hexagonal honeycomb under combined axial compression and transverse shear. Int J Solids Struct 2013;50:3934–46.
[21] Qiu C, Guan Z, Guo X, Li Z. Buckling of honeycomb structures under out-of-plane loads. J Sandw Struct Mater 2020;22:797–821.
[22] Pathirana ST. Local buckling analysis of composite corrugated and honeycomb structures. Washington: Washington State University; 2020. Ph.D Dissertation.
[23] Pathirana S, Qiao P. Elastic local buckling of periodic sinusoidal corrugated composite panels subjected to in-plane shear. Thin-Walled Struct 2020;157:107134.
[24] Pathirana S, Qiao P. Local buckling analysis of periodic sinusoidal corrugated composite panels under uniaxial compression. Compos Struct 2019;220:148–57.
[25] Composites L. In: Mechanics of Composite Structures. Cambridge: Cambridge University Press; 2003. p. 63–88.
[26] Qiao P, Huo X. Explicit local buckling analysis of rotationally-restrained orthotropic plates under uniform shear. Compos Struct 2011;93:2785–94.
[27] Kollár LP. Local buckling of fiber reinforced plastic Composite Structural Members with Open and Closed Cross Sections. J Struct Eng 2003;129:1503–13.
[28] Chen Q, Qiao P. Approximate closed-form solution for buckling of orthotropic plates with longitudinal edges elastically restrained against rotation. Thin-Walled Struct 2022;172:108688.
[29] Schreiber P, Mittelstedt C, Beerhorst M. Buckling of shear-deformable orthotropic laminated plates with elastic restraints. Thin-Walled Struct 2020;157:107071.
[30] Allen HG, editor. Analysis and design of structural sandwich panels: the commonwealth and international library: structures and solid body mechanics division. Elsevier; 2013.
[31] Zenkert D, Nordisk I. The handbook of sandwich construction. Cradley heath. West Midlands: Engineering Materials Advisory Services Ltd. (EMAS); 1997.
[32] Hohe J, Becker W. An energetic homogenisation procedure for the elastic properties of general cellular sandwich cores. Composites B 2001;32:185–97.
[33] Xia Z, Zhang Y, Ellyin F. A unified periodical boundary conditions for representative volume elements of composites and applications. Int J Solids Struct 2003;40:1907–21.
[34] ABAQUS, Software Package, Ver. 2019, Dassault Systemes Simulia Corporation.
[35] Wang R, Wang J. Modeling of honeycombs with laminated composite cell walls. Compos Struct 2018;184:191–7.
[36] Sriharan J, Dias M, Fernando D, Adhikari S. A unified approach for the prediction of the effective properties of laminated composite cellular core. Eng Struct 2024;299:117106.